

A NOVEL ROLE FOR HAPLN1 IN SKELETAL DEVELOPMENT

APPROVED BY SUPERVISORY COMMITTEE

Carol A. Wise, Ph.D.

Ondine Cleaver, Ph.D.

Bret Evers, M.D., Ph.D.

Makarand Risbud, Ph.D.

Ananth Madhuranthakam, Ph.D.

DEDICATION

To my mother and late father who have always been there for me.

To my mentor Dr. Carol Ann Wise who has taught me science is an art.

“People come into your life for a reason, a season, or a lifetime.”

-Brian Chalker

A NOVEL ROLE FOR HAPLN1 IN SKELETAL DEVELOPMENT

by

CHANDRESHKUMAR VISHNUBHAI PATEL

DISSERTATION

Presented to the Faculty of the Graduate School of Biomedical Sciences

The University of Texas Southwestern Medical Center at Dallas

In Partial Fulfillment of the Requirements

For the Degree of

DOCTOR OF PHILOSOPHY

The University of Texas Southwestern Medical Center at Dallas

Dallas, Texas

December, 2022

Copyright

by

Chandreshkumar Patel, 2022

All Rights Reserved

A NOVEL ROLE FOR HAPLN1 IN SKELETAL DEVELOPMENT

Chandreshkumar Vishnubhai Patel

The University of Texas Southwestern Medical Center at Dallas, 2022

Supervising Professor: Carol A. Wise, Ph.D.

Adolescent idiopathic scoliosis (AIS) is a potentially progressive spinal curvature that occurs during rapid growth and has a multi-factorial genetic etiology. Prior genetic studies in humans and animal models support differences in cartilage development in the pathogenesis of AIS. Here, we performed genome sequencing in families with inherited AIS and identified a co-segregating rare variant in the *HAPLN1* gene. *HAPLN1* encodes Hyaluronan and Proteoglycan Link Protein 1, also known as Cartilage Link Protein, that is reported to stabilize the extracellular matrix (ECM) by binding hyaluronic acid (HA) and proteoglycans in multiple tissues. One variant, p.C304S, was predicted to disrupt a critical disulfide bridge of the HAPLN1 C-terminal loop domain. In transient over-expression experiments, we detected wild type mouse Hapln1 protein in the cell lysate, media, and ECM, while Hapln1 p.C306S (C304S

in human) was detected in cell lysate and media, but not in the ECM. A truncated Hapln1 p.C306fs*5 (ET) lacking the C-terminal loop domain was detected only in the cell lysate. By mutagenesis experiments we found that replacing cysteines in Hapln1 primary disulfide bridges disrupted secretion and retention in the ECM, whereas replacing cysteines in secondary loops disrupted ECM retention only. Thus, all disulfide loops are required for ECM retention. Mice were engineered to harbor the orthologous mutations. While *Hapln1*^{ET/ET} mice died shortly after birth, exhibiting a chondrodysplastic phenotype with shortened limbs and dome-shaped head, *Hapln1*^{C306S/C306S} mice were viable, born at expected Mendelian ratios, and showed no significant skeletal malformations up to one year of age. Surprisingly, we were unable to detect Hapln1 protein in tissues of *Hapln1*^{C306S/C306S} mice although they were phenotypically normal. Furthermore, we found that *Hapln1* negatively regulates apoptosis in growth plate hypertrophic zones. Collectively, our data suggest an essential function for Hapln1 that is potentially independent of its role in the ECM.

TABLE OF CONTENTS

Prior Publications	ix
List of Figures	x
List of tables	xi
List of appendices	xii
List of definitions	xiii
Chapter One: Using genetics to identify rare variants	1
Definitive diagnosis of rare diseases using genome sequencing	1
The search for rare causal mutations in adolescent idiopathic scoliosis.....	2
Chapter Two: Review of the Literature	5
Human genetic studies	5
HAPLN1/Link Protein structure.....	6
HAPLN1/Link Protein role	7
Chapter Three: Methodology.....	11
Chapter Four: Results	24
Identifying new high-risk loci	24
C306S (human C304S) mutation in Hapln1 impairs its retention in the ECM <i>in vivo</i> ...	27
Cysteines are critical for the ECM retention of the Hapln1 protein	29
No colocalization between the Hapln1 protein and the cell membrane	32
<i>Hapln1</i> ^{C306S/C306S} mice appear normal, while <i>Hapln1</i> ^{ET/ET} mice display classic chondrodysplasia	34

Hapln1 protein is not detected in the growth plate of cartilage of <i>Hapln1</i> ^{C306S/C306S} mutant mice.....	38
<i>Hapln1</i> and <i>Col10a1</i> mRNA are expressed in growth plates of P0.5-day old <i>Hapln1</i> ^{C306S/C306S} mice, but greatly reduced in <i>Hapln1</i> ^{ET/ET} mice	42
<i>Hapln1</i> ^{ET/ET} mice have reduced proteoglycans and disorganized ECM	43
Apoptotic cells are increased in <i>Hapln1</i> ^{ET/ET} mice compared to <i>Hapln1</i> ^{C306S/C306S} and WT mice	45
μCT shows increased porosity in <i>Hapln1</i> ^{ET/ET} cortical bone	47
Chapter Five: Conclusions and Recommendations	49
Appendix.....	53
Bibliography	55

PRIOR PUBLICATIONS

Patel C, Khanshour AM, Wilkes D, Rios JJ, Sheff KW, Nassi L, Wise CA. Novel homozygous variant in WISP3 in a family with unrecognized progressive pseudorheumatoid dysplasia. *Clin Case Rep.* 2020;8(8):1452-7. Epub 2020/09/05. doi: 10.1002/ccr3.2884. PubMed PMID: 32884773; PMCID: PMC7455413.

Khanshour AM, Kou I, Fan Y, Einarsdottir E, Makki N, Kidane YH, Kere J, Grauers A, Johnson TA, Paria N, Patel C, Singhanian R, Kamiya N, Takeda K, Otomo N, Watanabe K, Luk KDK, Cheung KMC, Herring JA, Rios JJ, Ahituv N, Gerdhem P, Gurnett CA, Song YQ, Ikegawa S, Wise CA. Genome-wide meta-analysis and replication studies in multiple ethnicities identify novel adolescent idiopathic scoliosis susceptibility loci. *Hum Mol Genet.* 2018;27(22):3986-98. Epub 2018/11/06. doi: 10.1093/hmg/ddy306. PubMed PMID: 30395268; PMCID: PMC6488972.

LIST OF FIGURES

Figure 1. Relationship between frequency of human genetic variants and disease effect size	6
Figure 2. Genome sequencing strategy to identify candidate variants in subjects with AIS	26
Figure 3. Molecular modeling of the C304S (Cys-47) mutated protein.....	27
Figure 4. C306S (human C304S) mutation in Hapln1 impairs its retention in the ECM.....	29
Figure 5. Disulfide bridges are critical for ECM retention of Hapln1 protein	31
Figure 6. Pull-down of biotinylated membrane proteins show no co-localization of Hapln1 protein on the cell membrane.....	33
Figure 7. <i>Hapln1</i> ^{C306S/C306S} and <i>Hapln1</i> ^{ET/ET} mutant lines generated via CRISPR show chondrodysplastic phenotype in <i>Hapln1</i> ^{ET/ET} mice.....	36
Figure 8. H&E of P0.5-day old <i>Hapln1</i> ^{ET/ET} mice show complete disorganization of the IVD and femur.	37
Figure 9. Validation of the monoclonal anti-Hapln1 antibody	40
Figure 10. Hapln1 is undetected in <i>Hapln1</i> ^{C306S/C306S} and <i>Hapln1</i> ^{ET/ET} mice	41
Figure 11. <i>Hapln1</i> and <i>Coll10a1</i> mRNA is expressed in the growth plate of P0.5-day old <i>Hapln1</i> ^{C306S/C306S} and WT mice while <i>Hapln1</i> ^{ET/ET} mice show reduction in their levels.....	43
Figure 12. The growth plate of <i>Hapln1</i> ^{ET/ET} mice shows reduction in total proteoglycan levels, Aggrecan, and Collagen X compared to WT and <i>Hapln1</i> ^{C306S/C306S} mice.....	45
Figure 13. The growth plate of <i>Hapln1</i> ^{ET/ET} mice shows an increase in cells positive for apoptosis compared to WT and <i>Hapln1</i> ^{C306S/C306S} mice.....	47
Figure 14. <i>Hapln1</i> ^{ET/ET} mice show malformation of bone in p0.5 days old mice	48

LIST OF TABLES

Table 1- Schematic for construction of Hapln1 clones..... 13

Table 2- HAPLN1 mutations identified in WGS and WES screen 25

LIST OF APPENDICES

Appendix A-JIA-WISP3 study 53
Appendix B-AIS-GWAS study..... 54

LIST OF DEFINITIONS

AIS – Adolescent idiopathic scoliosis

ECM – Extracellular matrix

HA – Hyaluronic acid

IVD – Intervertebral disc

RT – Room temperature

μ CT – micro-computed tomography

WT – Wild Type

H&E – Hematoxylin & Eosin

TUNEL – Terminal Deoxynucleotidyl Transferase (TdT)-Mediated dUTP Nick-End

Labeling

JIA – Juvenile Idiopathic Arthritis

GWAS – Genome wide association studies

WGS – Whole genome sequencing

WES – Whole exome sequencing

P0.5 – postnatal day 0.5

P28 – postnatal day 28

CHAPTER ONE

Using genetics to identify rare variants

Definitive diagnosis of rare diseases using genome sequencing

I have been a student at the University of Texas Southwestern Medical Center in the Biomedical Engineering graduate program and on the Mechanisms of Disease and Translational Science (MoDTS) Graduate Track. The latter track emphasizes translational research and has two aims. The first aim is to allow Ph.D. students to shadow physicians to observe diagnostics, therapeutics, and procedures in a clinical setting. The second aim of this track is to work with the physicians on a clinical research project that “bridges the gap” between bench and bedside. During this track I shadowed the rheumatology clinic at Scottish Rite for Children, under the mentorship of Dr. Tracey Wright. For the bench to bedside project, under the mentorship of Dr. Lorien Nassi, I worked on a project involving a patient who initially presented with classical signs of Juvenile Idiopathic Arthritis (JIA) but was resistant to treatment. JIA is the most common form of arthritis in children, with clinical symptoms presenting as stiffness, effusion, and limited range of motion. As implied by the name, JIA describes a group of heterogeneous disorders that are diagnosed by exclusion of other disorders with similar presentations (Kim & Kim, 2010). The etiologies underlying JIA are unknown. The diagnosis of JIA is challenging, as a number of other musculoskeletal diseases such as idiopathic multicentric osteolysis, mucopolysaccharidosis, camptodactyly-arthropathy-coxa vara-pericarditis syndrome, and progressive pseudorheumatoid dysplasia mimic the presentation of JIA. However, unlike JIA, these conditions are noninflammatory in nature (Al-

Mayouf, 2018). Misdiagnosis of patients with symptoms resembling JIA delays correct diagnosis leading to inappropriate and/or unnecessary treatment. Dr. Nassi had noted that the patient had an affected sibling who was also resistant to treatment. Consequently, we speculated that their disease was heritable. By applying genomic methods, we discovered that both patients had inherited a novel loss-of-function (LOF) mutation in the *WISP3* gene from each parent. The presence of homozygous LOF mutations was consistent with a diagnosis of progressive pseudorheumatoid dysplasia. This case study was unique, as radiographic imaging showed signs of effusion in the patient that is characteristic of JIA but not previously associated with progressive pseudorheumatoid dysplasia. A published report of our study can be found in **Appendix A**.

The search for rare causal mutations in adolescent idiopathic scoliosis

Scoliosis is a complex, 3-dimensional disorder with both a lateral and rotational deformity of the spine. There are four major types of scoliosis: congenital, idiopathic, neuromuscular, and syndromic, with idiopathic scoliosis being the most prevalent. An “idiopathic” diagnosis is one of exclusion, made only when other causes of scoliosis are ruled out. Idiopathic scoliosis (“IS”) is the most common pediatric musculoskeletal disorder, with a population prevalence of 2-3% and affecting over 29 million children worldwide (Rogala, Drummond, & Gurr, 1978). Idiopathic scoliosis is further classified into one of three subcategories based on the age of onset: infantile (on set 0-3 years of age), juvenile (JIS, on set 4-9 years of age), or adolescent (AIS, on set 10 years and older) (Akbarnia, 2007). Adolescent Idiopathic Scoliosis (AIS) is the most common form of IS, representing over 75% of all IS diagnoses. In AIS, the progression

of the spinal deformity correlates with the adolescent growth spurt (Little, Song, Katz, & Herring, 2000). There is significant sexual dimorphism in the expression of AIS, with females being at least five times more likely to have progressive scoliosis that requires treatment, and ten times more likely to require surgical correction (Karol, Johnston, Browne, & Madison, 1993). If left untreated, AIS can lead to spinal curve progression with severe deformity later in life, restrictive lung disease, cardiopulmonary problems, psychosocial issues, and pain (Asher & Burton, 2006; Haller et al., 2016; Herring, 2008; Hresko, 2013; Stuart L. Weinstein, Dolan, Cheng, Danielsson, & Morcuende, 2008). Treatment for AIS is symptomatic, with the patient initially being monitored radiographically to measure the progression of the curve. Progression of the curve before peak growth velocity is a predictor of serious deformity (Little et al., 2000). The purpose of bracing is to prevent the progression of the curve, without expectation that it will correct existing deformity. While randomization time-in-brace studies suggest that bracing is effective, about 10% of those patients will continue to progress and require surgical correction (Asher & Burton, 2006; Katz, Herring, Browne, Kelly, & Birch, 2010; Sanders et al., 2014; S. L. Weinstein, Dolan, Wright, & Dobbs, 2013). Corrective surgery typically involves posterior spinal fusion of 6 to 10 vertebrae, with an implantation of metal instrumentation to straighten the spine (Carragee & Lehman, 2013). Complications following surgery can be neurological damage, infection, venous thromboembolism, gastrointestinal complications, implant-related complication, spinal cord injury, and long-term loss of spinal motion (Chan et al., 2002; Hresko, 2013; Murphy & Mooney, 2016). The estimated hospital costs of operative treatment for AIS exceeds one billion USD annually (Gao et al., 2007;

Martin et al., 2014; Salehi et al., 2002). Thus, the morbidity, impact to families, and costs of treating AIS poses a significant health burden worldwide.

As the name implies, the causes of AIS are largely unknown. Familial segregation studies support a multifactorial, or complex inheritance model of AIS susceptibility, in which multiple genetic factors increase risk of the disease in individual patients (Riseborough & Wynne-Davies, 1973; Tang et al., 2012). Multiple AIS risk loci have been identified, mostly by genome-wide association studies (GWAS) (Khanshour et al., 2018; Ogura et al., 2018; Sharma et al., 2015; Wise et al., 2020). Recently, our laboratory led an international meta-analysis of existing GWAS that validated prior findings and replicated new loci associated with AIS (published report attached as **Appendix B**). Gene set enrichment analysis of that dataset (N=33,476 individuals) underscored genes involved in cartilage/connective tissue biogenesis (Khanshour et al., 2018). In my thesis project, we sought to define novel genetic variants conferring high risk of AIS by studying multiply affected families. In our study we applied knowledge gained in our prior studies and restricted our focus to genes involved in cartilage development and/or homeostasis. To identify these variants, we obtained whole genome sequencing (WGS) and performed variant filtering in a unique cohort of families with dominantly inherited AIS. Here I will show *in vitro* and *in vivo* results from the functionalization of variants in one high priority candidate gene, *HAPLN1*, discovered through this screen.

CHAPTER TWO

Review of the Literature

Human genetic studies

As noted, AIS is a complex multifactorial disease. Most “gene discovery” for AIS has been via GWAS, a method that has already yielded a number of common genetic risk loci for AIS (Wise et al., 2020). In brief, GWAS is an analysis method in which polymorphisms, typically single nucleotide polymorphisms, or “SNPs” are genotyped in populations ascertained for the diagnosis of interest. The frequency of each SNP allele in the affected population is compared to its frequency to the control population. Those alleles that show statistically significant differences (after correcting for multiple testing, and independent validation), become markers of risk loci in the genome (Paria et al., 2013). A GWAS meta-analysis published by our group highlighted variants in or near genes involved in cartilage and connective tissue development in AIS (Khanshour et al., 2018; Wise et al., 2020). While GWAS is statistically robust at identifying genotype-phenotype associations for common variants it typically lacks the ability to assess very rare genetic variants, which are expected to convey a higher disease risk and greater heritability (Figure 1). Complex multifactorial diseases, such as AIS, may be caused by both rare, high penetrance, and common, low to medium penetrance variants in the genome (Antonarakis, Chakravarti, Cohen, & Hardy, 2010). Consequently, it is important to identify both common and rare variants to fully define the underlying AIS disease mechanisms. To identify rare high impact variants for AIS we obtained whole genome sequencing (WGS) from 72 multiply affected families with dominant AIS. This work was supported by Gabriella Miller

Kids First (GMKF) Pediatric Research program grant # X01HL132375. Analysis of WGS in the 72 families was performed by Dr. Anas Khanshour in our group as outlined in the Results section below. By filtering for protein-altering sequence variants in cartilage genes, we identified *HAPLN1* as a potential AIS candidate gene.

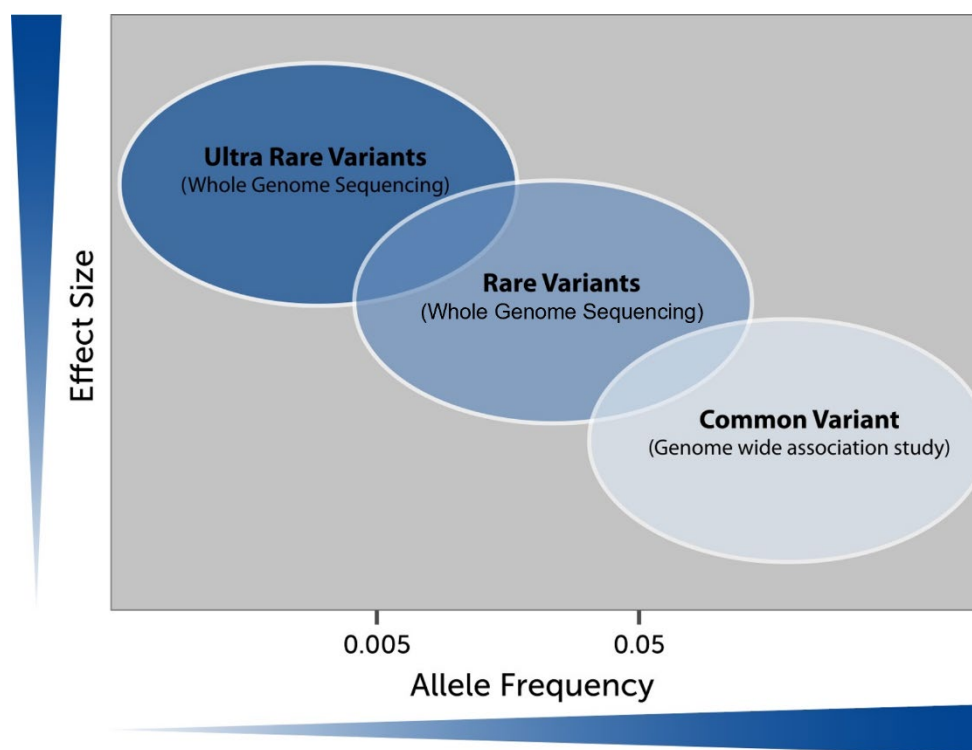


Figure 1. Relationship between frequency of human genetic variants and disease effect size. The benefits of using GWAS, and WGS to identify common, rare, and ultra-rare variants is conceptualized in this cartoon.

HAPLN1/Link Protein structure

HAPLN1, Hyaluronan And Proteoglycan Link Protein 1, also known as *CRTL1*, Cartilage Link Protein 1, is a small gene consisting of five exons. Exon 1 contains the 5' untranslated region (UTR), exon 2 encodes the signal peptide and N-terminal peptide, exon 3 encodes an aggrecan binding module, A, exon 4 encodes the first hyaluronic acid (HA) binding module B, and exon 5 encodes for the second HA binding module B' of *HAPLN1* (Figure 2A) (Grover & Roughley,

1994). A previously published study examined the interaction of HAPLN1 binding to HA. In that analysis, mutant constructs with either the B, or B' loops removed was created and expressed *in vitro* in a baculoviral system and tested for interaction with HA. The results revealed that mutant constructs containing only one of the HA binding domains B or B', individually still retained the ability to interact and bind to HA *in vitro* (Grover & Roughley, 1994). The HAPLN1 protein has five disulfide bonds, one in the aggrecan binding domain A, and two in each of the hyaluronan (HA) binding domains B and B' (Blundell et al., 2005; Grover & Roughley, 1994; Mahoney, Blundell, & Day, 2001). While the vertebrate HAPLN family (HAPLN1-4) shares only 45-52% amino acid identity, all ten cysteine residues are conserved across the family (Spicer, Joo, & Bowling, 2003). In human neonates three distinct forms of HAPLN1 can be detected: (1) intact HAPLN1 with a single N-terminal oligosaccharide at residue 41, (2) two N-terminal oligosaccharides at residues 6 and 41, or (3) a proteolytically cleaved form, in which a N-terminal, 16 amino acid peptide is removed (Figure 2B) (Nguyen, Liu, Roughley, & Mort, 1991). This 16-amino acid fragment, called "N-link" peptide has been proposed to stimulate the production of proteoglycans *in vitro* (Wang, Weitzmann, Sangadala, Hutton, & Yoon, 2013). Specifically, human N-link peptide induced expression of SOX9, aggrecan, and collagen II, in cells isolated from the intervertebral disc (IVD) of rabbits grown in a three-dimensional alginate bead matrix (Wang et al., 2013). The study further suggested that the N-link peptide binds and activates the Bone Morphogenetic Protein (BMP) Type II Receptor (Wang et al., 2013).

HAPLN1/Link Protein role

The HAPLN1 protein is expressed in cartilage, heart, lung, and brain, where it is proposed to be responsible for the formation and stabilization of proteoglycans in the ECM. In cartilage and IVD, the ECM consists of collagens, which provide tensile strength, and proteoglycan aggregates which retain water, providing osmotic pressure and resistance to compression (H. Y. Watanabe, Yoshihiko, 2003). Aggrecan, HA, and HAPLN1 are major components of these aggregates. In cartilage the ECM can account for approximately 90% of the tissue by dry weight, with aggrecan being the most abundant form of proteoglycan present (Kiviranta, Jurvelin, Tammi, Säämänen, & Helminen, 1985; Kornak & Mundlos, 2003). In the IVD, proteoglycans account for ~65% of the nucleus pulposus and ~20% of the annulus fibrosus by dry weight (Gruber et al., 2011). Newly synthesized aggrecan is thought to undergo a conformational change before binding to HA. Binding to the HAPLN1 domain A is proposed to accelerate that conformational change, allowing for dense packaging of aggregates in the ECM (Nguyen et al., 1991; Rodriguez & Roughley, 2006; Roughley, 2006). The remaining two link modules B and B' tether it to the HA chain. The first link module, B, binds to six HA oligosaccharides while the second link module, B', binds to four HA oligosaccharides (Blundell et al., 2005). Together the HAPLN1 binds aggrecan along the long HA chain in a 1:1 stoichiometric ratio. Thus, the primary role attributed to HAPLN1 protein is thought to be its tight packing of aggrecans along the HA chain in the ECM, preventing their dissociation under physiological conditions (Rodriguez & Roughley, 2006; Roughley, 2006). The HAPLN1 Protein also coats the HA strand and presumably protects it from degradation (Rodriguez & Roughley, 2006; Roughley, 2006).

Germline knockouts of the proteoglycan genes encoding, *Hapln1*, Aggrecan (*Acan*), or HA (*Has2*) are each lethal in mice (Camenisch et al., 2000; Roughley, 2006; H. Watanabe, Nakata, Kimata, Nakanishi, & Yamada, 1997; H. Y. Watanabe, Yoshihiko, 2003). Knockout of the aggrecan encoding gene, *Acan*, in mice is perinatal lethal and displays the phenotype of cleft palate, dwarfism (short limbs, tail, and a short snout) (H. Watanabe et al., 1997; H. Y. Watanabe, Yoshihiko, 2003). While heterozygous *Acan* mice appear normal at first, within two months they display slight dwarfism and by 12 months of age they develop hyperlordosis of the spine (H. Watanabe et al., 1997; H. Y. Watanabe, Yoshihiko, 2003). Knockout of the *Has2* gene in mice resulted in embryonic death around E9.5-10 prior to skeletal development (Roughley, Lamplugh, Lee, Matsumoto, & Yamaguchi, 2011). Knockout of *Hapln1* in mice is perinatal lethal, phenocopying *Acan* KO, with animals exhibiting severe chondrodysplasia (Czipri et al., 2003; H. Watanabe et al., 1997; H. Watanabe & Yamada, 1999; H. Y. Watanabe, Yoshihiko, 2003). In these animals the chondrocytes in the growth plates of the limbs, vertebral bodies, and IVD were severely disorganized, with a few surviving mice developing lordosis of the spine (Czipri et al., 2003; H. Watanabe & Yamada, 1999). Expressing a *Hapln1* transgene driven by a *Col2A1* promoter rescued perinatal lethality. In fact, animals expressing as low as 20% of wild type protein levels survived to adulthood. The mice however were smaller, displayed severe chondrodysplasia, and developed hyperlordotic and hyperkyphotic curvature along the thoracic spine (Czipri et al., 2003). The authors of these studies concluded that low level expression in osteochondral progenitor cells was sufficient to rescue lethality, although mis-expression from the *Col2A1* promoter could not be ruled out (Czipri et al., 2003). *Hapln1* KO mice have been noted to phenocopy mice lacking *Coll1a1* (Li et al., 1995), a gene

with variants we have also associated with AIS (unpublished). Thus, we hypothesized that the novel HAPLN1 mutations identified in AIS patients may confer functional changes that could lead to an AIS phenotype. To study these mutations, we performed the experiments described in the Results section.

CHAPTER THREE

Methodology

Animal studies

All the animal studies were performed according to the University of Texas Southwestern Medical Center Institutional Animal Care and Use Committee (IACUC) guidelines and regulations. The IACUC protocols were reviewed and approved under the IACUC Protocol No: 2016-101455.

Sequencing

Human subjects were previously recruited per protocol STU 112010-150 as approved by the University of Texas Southwestern Medical Center Institutional Review Board. WGS of 287 individuals from 72 families with dominantly inherited AIS was performed using Illumina paired-end sequencing followed by standard quality control and variant calling and annotation measures. Variants were filtered for rare protein-altering changes with minor allele frequency (MAF) $\leq 1\%$ in Genome Aggregation Database (gnomAD), then further prioritized for co-segregation with AIS in at least 2 independent families and a reported biological role in cartilage development.

Generation of mouse Hapln1 mutants

Hapln1^{C306S}, and Hapln1^{C306fs*5(ET)} were generated using CRISPR/Cas9 gene editing. Briefly, a guide RNA (gRNA), gRNA: ATCCTATTTCTCGACCAAGAAGG, with the protospacer

adjacent motif (PAM) site in bold, was designed with a donor sequence GAAAGTGGGCCAGATATTTGCTGCCTGGAAGCTTCTGGGCTATGACCGCT**TCCGA** TGCCGGCTGGCTAGCGGATGGCAGCGTCCGCTATCCTATTTCTCGACCAAGA**AG** ACGCTGCAGTCCGACTGAGGCTGCAGTGC**GCTTTGTAGGTTTCCCAGATAA** to target the TGC codon encoding the C306 amino acid. The TGC codon was mutated to TCC, bolded in the donor sequence, to create the C306S mutation. A synonymous mutation was also inserted into the PAM site, AGG to AGA, bolded in the donor sequence, to prevent CRISPR/Cas9 from re-cutting (Figure 7A). The early termination (ET) mutation was created by deletion of the guanine nucleotide in the same TGC codon, causing a frameshift and early termination of the Hapln1 protein. To mitigate the risk of off -target effects, each line was bred out to WT for three generations prior to being used for experimental purposes. Mice were genotyped by enzymatic digestion. Briefly, mice were genotyped by PCR using the forward primer TGGTTCATCACAGGCTGAC, and the reverse primer TGGCCTTTATGAAAACGACTC resulting in a 487-base pair (bp) product. Introduction of the C306S and ET mutation altered the sequence, creating a MbiI restriction enzyme site. To genotype the mice the PCR product was digested by FastDigest MbiI (ThermoFisher, cat. no. FD1274), WT resulted in no digestion, a single 486bp product, creating three products, 487bp, 176bp, and 311bp products in heterozygous animals, and 176bp and 311bp products in homozygous animals. Results of genotyping were validated by Sanger sequencing.

Mutagenesis

Mouse Hapln1 (NM_013500) Mouse Tagged ORF Clone (Origene, CAT#: MR205436) was used to create additional mutants. Mutated nucleotides and their corresponding amino acid change are shown in Table 1. Briefly, mutagenesis primers were designed using the Takara website (<https://www.takarabio.com/learning-centers/cloning/primer-design-and-other-tools>). Clones were created using In-Fusion HD Cloning Plus (Takara, cat. no. 638910) following the manufacture's protocol and introduced into Invitrogen One Shot TOP10 Chemically Competent E. coli (ThermoFisher, cat. no. C404003). All Clones were verified by Sanger sequencing.

Loop	Nucleotide change	Amino Acid change
B'	G1012A	G338S
B'	C995G	P319A
B	G548C	C183S
B	G620C	C207S
B	G683C	C228S
B	G761C	C254S
B'	G842C	C281S
B'	G917C	C306S
B'	G980C	C327S
B'	G1052C	C351S
B'	G917del	C306fs*5

Table 1. Schematic for construction of Hapln1 clones. Location, nucleotide and resulting amino acid changes.

Transfection and immunofluorescence of COS-7 cells

Coverslips were placed in each well of a 6 well plate. COS-7 (ATCC, Cat no. CRL-1651) cells were seeded at a density of 250k cells into each well. Cells were transfected after 24 hours using Promega FuGENE HD Transfection Reagent (Promega, Madison, WI, Cat no. E2311). Transfections were done with a FuGENE HD Transfection Reagent(uL) to DNA(μ g) ratio of 3:1 with 6 μ L of FuGENE HD to 3 μ g plasmid. After 48 hours cells were washed three times

with phosphate buffered saline (PBS). Cells were then fixed in 4% formaldehyde for 15 minutes at room temperature (RT) followed by three washes in PBS for 5 minutes each. Cells were permeabilized in ice-cold 100% methanol for 10 minutes at -20°C followed by three washes in PBS for 5 minutes each. Cells were blocked in 3% bovine serum albumin (BSA) (Sigma-Aldrich, cat. no. A7906-100G) in PBS for 1 hour at RT, then incubated with rabbit anti-Na,K-ATPase $\alpha 1$ (Cell Signaling, cat. no. 23565S) at 1:100 dilution and mouse anti-Myc (Cell Signaling, cat. no. 2276S) at 1:200 dilution or mouse monoclonal anti-Hapln1 (Developmental Studies Hybridoma Bank, Iowa, 9/30/8-A-4) at 5 μ g/mL and rabbit anti-Myc (Cell Signaling, cat. no. 2272S) at 1:200 dilution over night at 4°C. After 24 hours cells were washed three times with PBS for 5 minutes each followed by incubation with Goat anti-Mouse Alexa Fluor 488 (ThermoFisher, cat. no. A-11029) and Goat anti-Rabbit Alexa Fluor 594 (ThermoFisher, cat. no. A-11012) at 1:500 dilution each for 1 hour at RT. Cells were then washed three times with PBS for 5 minutes each followed by mounting on slide with VECTASHIELD HardSet Antifade Mounting Medium With 4',6-diamidino-2-phenylindole (DAPI) (Fisher Scientific, cat. no. NC9029229). Slides were imaged using Zeiss LSM880 and Zeiss Axio Imager.M2.

Fractionation and Western blot

250k HEK 293T cells were plated in a 6 well plate overnight. The next day cells were transfected as described above with FuGENE HD Transfection Reagent:DNA, ratio of 3:1, with 6 μ L of FuGENE HD to 3 μ g plasmid. After 24 hours, media was removed, and fresh Opti-MEM I Reduced Serum Medium (Fisher Scientific, cat. no. 31-985-062) was added to the

cells. After 24 hours, cell lysate, media, and ECM fractions were collected. Due to their low adherence to the 6-well plates HEK 293T cells can be lifted off the plate with gentle agitation by pipetting the media until the cells have come off. The media containing the cells was spun at 1000 g for 10 minutes. The supernatant (cell media) was saved and the pellet containing cells was lysed using Radioimmunoprecipitation assay (RIPA) Lysis and Extraction Buffer (Fisher Scientific, cat. no. PI89900) with Halt Protease Inhibitor cocktail (Fisher Scientific, cat. no. PI87786) added in, on ice for 30 minutes. The cell lysate was then spun down at 12,000 rpm for 10 minutes at 4°C and the supernatant (cell lysate) was saved. The media saved from earlier was further concentrated using an amicon ultra-4 with a 10KDa cutoff (Millipore Sigma, cat. no. UFC801024) at 4,000 g for 30 minutes at 4°C. The 6-well plate was washed 3 times with PBS ensuring no cells were still attached to the plate. The ECM was then extracted directly from the 6-well plate in 30µL RIPA buffer with Halt Protease Inhibitor cocktail. Cell lysate, cell media, and ECM were further diluted 1:4 in NuPAGE LDS Sample Buffer 4X (ThermoFisher, cat. no. NP0007) prior to denaturing at 95°C for 10 minutes. All samples, cell lysates, the concentrated media, and ECM were loaded onto SurePAGE, Bis-Tris, 4-20% gradient gel (GenScript, cat. no. M00657) and electrophoresed at 100V for 90-120 minutes. The protein was transferred onto an Odyssey nitrocellulose membrane (Li-Cor, cat. no. 926-31090) at 100V for 1 hour. The membrane was blocked for 1 hour in Intercept Tris-Buffered Saline (TBS) blocking buffer (Li-Cor, cat. no. 927-60001). The membrane was probed with Myc-anti rabbit (1:1000) (Cell Signaling, cat. no. 2272S) or mouse monoclonal anti-HAPLN (Developmental Studies Hybridoma Bank, Iowa, 9/30/8-A-4) at 0.5µg/mL overnight in the Intercept T20 (TBS) Antibody diluent buffer (Li-Cor, cat. no. 927-65001) at 4°C on a rocker.

Next day the membrane was washed three times with TBS with 0.2% Tween 20 (Fisher Scientific, BP337-500) (TBST) for 10 minutes each with the final wash in TBS alone. The membrane was then probed with the secondary antibodies IRDye 680RD Goat anti-Rabbit (Li-Cor, cat. no. 926-68071) or IRDye 680RD Goat anti-Mouse (Li-Cor, cat. no. 926-68070) for 1 hour, then washed three times in TBST with the final wash in TBS alone. Additionally, the membrane was probed with GAPDH Loading Control Monoclonal Antibody (GA1R), DyLight 800 4X PEG (ThermoFisher, MA5-15738-D800) at 1:3000 dilution for 1 hour. Membranes were analyzed using the Li-Cor Odyssey FC imaging system.

Immunohistochemistry

Immunohistochemistry (IHC) was performed on postnatal day 0.5 (P0.5) mouse pups. Whole pups, spines, or legs were fixed in 4% neutral buffered formalin for 72 hours. After fixation tissue was dehydrated and cleared in a tissue processor (Leica, Leica ASP300S). Tissues were paraffin embedded with no decalcification. Tissues were sectioned at 4 μ m on APES, (3-aminopropyl)triethoxysilane, (Sigma-Aldrich, A3648-100mL) treated microscope slides and allowed to dry overnight. Slides were heated at 65°C for 1 hour followed by deparaffinization by three changes in xylene for 5 minutes each and rehydrated in descending grade of alcohol for 3 minutes each, immediately followed by washing in distilled water. Antigen retrieval was performed using hyaluronidase (Sigma-Aldrich, H3506-1G), 2mg/mL or 25mg/mL, at 37°C for 30 minutes or 1 hour. Slides were then washed in distilled water. Endogenous peroxidase was blocked by placing the slides in a final concentration of 3% H₂O₂ in methanol for 10 minutes followed by three changes in distilled water before transferring the slides to PBS.

Slides were blocked with 10% goat serum (normal) (Dako, X0907) in PBS for 1 hour at RT, then incubated with the primary antibody mouse monoclonal anti-Hapln1 (Developmental Studies Hybridoma Bank, Iowa, 9/30/8-A-4) at 5µg/mL, rabbit polyclonal anti-Aggrecan (Sigma-Aldrich, AB1031) at 1:100 dilution, or rat polyclonal anti-Type X Collagen (Cosmo Bio Co., LTD, LSL-LB-0092) at 1:50 dilution, overnight at 4°C. Slides were then washed three times for 5 minutes each in PBS with 0.1% tween 20, then incubated for 1.5 hours with, Goat anti-Mouse-HRP (Millipore, AP181P), Goat anti-Rabbit-HRP (Millipore, AP187P), or Goat anti-Rat-HRP (Millipore, AP136P) at 1:500 dilution in PBS at RT. Afterwards, slides were washed three times for 5 minutes each in PBS with 0.1% tween 20. Excess solution was washed off and slides were probed with DAB chromogen (Agilent Technologies, Inc., K3468) for a maximum of 10 minutes, then immediately washed with distilled water. Nuclei were counterstained with Mayer's hematoxylin for 1 minute and washed in running water for 3 minutes. Slides were then dehydrated in ascending grade of alcohol followed by three washes in xylene. Slides were mounted using Eprelia Cytoseal XYL (Fisher Scientific, 22-050-262) and imaged using Olympus BX63.

Immunofluorescence

Immunofluorescence (IF) was performed similar to the above IHC protocol. Tissues were fixed, embedded, and sectioned using the protocol above. Slides were deparaffinized and rehydrated in descending grade of alcohol as described in the above IHC protocol. Antigen retrieval was performed using hyaluronidase, 2mg/mL or 25mg/mL, at 37°C for 30 minutes to 1 hour, followed by washing in PBS. Slides were then blocking in 10% normal goat serum in

PBS for 1 hour at RT. Slides were incubated with the primary antibody mouse monoclonal anti-Hapln1 (Developmental Studies Hybridoma Bank, Iowa, 9/30/8-A-4) at 5 μ g/mL, rabbit polyclonal Aggrecan (Sigma-Aldrich, AB1031) at 1:100, or rat polyclonal anti-Type X Collagen (Cosmo Bio Co., LTD, LSL-LB-0092) at 1:50 dilution, overnight at 4°C. Slides were then washed three times for 5 minutes each in PBS with 0.1% Tween 20. Donkey anti-Mouse-594 (Invitrogen, A-21203), Donkey anti-Rabbit-594 (Invitrogen, A-21207), or Donkey anti-Rat-594 (Invitrogen, A-21209) was added at 1:250 dilution in PBS to the slides for 1 hour at RT. Slides were then washed 3 times for 5 minutes each in PBS with 0.1% Tween 20. Slides were mounted using antifade mounting medium with DAPI (Vectashield, H-1200). Slides were imaged using Zeiss LSM880 and Zeiss Zeiss Axio Imager.M2.

RNA Scope

RNAscope chromogenic assay was used to detect transcript for *Hapln1* and *Col10a1* genes in paraffin-embedded tissues. The probe for mouse Hapln1 was targeted to the region 151-1143, Accession No: NM_013500.4, (ACD, Newark, CA, Cat No. 448201). Probe for mouse Col10a1 was targeted to the region 1616-2796, Accession No: NM_009925.4, (ACD, Newark, CA, Cat No. 426181). Slides were deparaffinized and pretreated following the manufacturer's instructions (Advanced Cell Diagnostics, Inc (ACD), California). Briefly, slides were boiled in Target Retrieval solution, followed by rinsing the slides in distilled water (dH₂O) and dehydrating in 100% ethanol. Enzymatic digestion was performed at 40 °C for 15 minutes. Hybridization was performed following the manufacture's procedure using the reagents for RNAscope 2.5 HD Detection Kit-RED (ACD, cat # 322360). The probes (Mm-Hapln1

cat# 448201 and Mm-Col10a1 cat# 426181) were applied to the slides at 40 °C for 2 hours. Amplification steps were done following the manufacturer's instructions. Lastly, chromogenic signal detection (red) was achieved using a mix of Fast RED-B and Fast RED-A in a ratio of 1:60 at room temperature for about 10 minutes. Slides were then washed in dH₂O and counterstained with hematoxylin before applying ECoMount mounting medium (BioCare Medical, SKU:EM897L) and a coverslip over the tissue section. Slides were imaged using Zeiss Axio Imager.M2.

TUNEL Assay

Tissues of P0.5 femoral bone was paraffin processed, embedded, and sectioned as described in the IHC methods. Serial paraffin sections were collected for the region of interest. Apoptotic cells were detected using Promega DeadEnd Fluorometric TUNEL System (Promega, cat. no. G3250). Terminal Deoxynucleotidyl Transferase (TdT)-Mediated dUTP Nick-End Labeling (TUNEL) assay was performed using manufacture's protocol. Positive apoptotic cells were labeled with fluorescein-12dUTP supplied with the DeadEnd Fluorometric TUNEL System. Sections were further counterstained with propidium iodide. Slides were imaged using Zeiss Axio Imager.M2.

Safranin O staining for cartilage

Similar to the other staining protocol, femurs of P0.5-day old pups was paraffin processed, embedded, and sectioned as describe in the IHC methods. Tissue slides were deparaffinized, hydrated, and washed under running water. Slides were then stained in Weigert's hematoxylin

for 10 minutes immediately following another wash in running water for an additional 5 minutes. Slides were quickly placed in acid alcohol, 1% hydrochloric acid in 70% alcohol, for 15 seconds, then washed in water for 5 minutes following staining in aqueous Fast green (0.1% (weight/volume) Fast green in dH₂O) for 3 minutes following a brief wash in 1% acetic acid. Afterwards, slides were stained in 0.1% (w/v) Safranin O in dH₂O for 3 minutes, followed by rinsing in 95% alcohol. Finally, slides were dehydrated in ascending grade of alcohol to three changes in xylene and mounted using EpreDia Cytoseal XYL (Fisher Scientific, 22-050-262). Slides were imaged using Olympus BX63.

Hematoxylin & Eosin (H&E) staining

Tissue slides were deparaffinized and hydrated as described above, then stained in Mayer's hematoxylin for 5 minutes immediately after rinsing in tap water. Slides were then placed in Eosin for 5 minutes, then washed in water than dehydrated in ascending grade of alcohol to finally three changes in xylene. Finally, slides were mounted using EpreDia Cytoseal XYL (Fisher Scientific, 22-050-262), and imaged using Olympus BX63.

Whole-Mount Skeletal Staining

P0.5-day old pups were sacrificed by opening of the abdominal cavity under deep anesthesia via hypothermia, followed by submersion in cold fixative. Skin, internal organs, eyes, and adipose tissue was removed. Mice were then fixed in 95% ethanol overnight at RT. The next day mice were placed in acetone overnight at RT. Cartilage was stained by submerging the skeleton in Alcian blue, 0.03% (weight/volume) in 200 proof ethanol, 80%, and (glacial) acetic

acid, 20%, overnight at RT. Skeletons were then washed in two changes of 70% ethanol before incubating in 95% ethanol overnight at RT. The samples were then pre-cleared in 1% potassium hydroxide (KOH) in dH₂O for 1 hour at RT. The KOH solution was removed, and the samples were then submersed in an Alizarin red solution, 0.005% (weight/volume) in 1% KOH solution, for 3-4 hours at RT. To clear excessive Alizarin red solution, samples were placed in a 50% glycerol:50% (1%) KOH solution. Samples were placed in 100% glycerol for long-term storage (Rigueur & Lyons, 2014).

μCT of mice

Mice were euthanatized under CO₂ with a heart puncture as a secondary measure at 6 months of age. Prior to fixation the femur and tibia were cleaned by removing as much soft tissue as possible. Skeletons were then fixed in a 4% paraformaldehyde solution for two days. The bones were dissected and kept in 70% alcohol for storage. Micro-computed tomography was performed by Dr. Aysha Khalid in our group using a Skyscan 1072 X-ray Microtomograph (Skyscan, Aartselaar, Belgium) set at 50kV/ 200μA. After ensuring the bone was within the scout view, images were acquired at 8-μm resolution with a rotation step of 0.4°. Reconstruction of the three-dimensional models was done using NRecon version 1.7.4.6 (Skyscan), with the trabecular parameters measured using Skyscan recommended methods. The analysis of the trabecular bone was calculated on 200 slices from the region just below the growth plate with a threshold of 63-255 using American Society of Bone and Mineral Research nomenclature. Similarly, the cortical parameters were calculated on 200 slices from a region just below the growth plate with a threshold of 114-255.

Colocalization study

COS7 cells were transfected and stained as described in the transfection and immunofluorescence of COS-7 cells methods section. Briefly, cells were probed for rabbit anti-Na,K-ATPase $\alpha 1$ (Cell Signaling, cat. no. 23565S) with secondary Goat anti-Rabbit Alexa Fluor 594 (ThermoFisher, cat. no. A-11012) paired with mouse anti-Myc (Cell Signaling, cat. no. 2276S) with secondary Goat anti-Mouse Alexa Fluor 488 (ThermoFisher, cat. no. A-11029). Immunofluorescence z-stack images of COS-7 cells transfected with WT, *Hapln1*^{C306S} or *Hapln1*^{ET} were collected. Colocalization analysis was performed using Imaris x64 version 9.5.1. Images were converted to .IMS files and opened using Imaris. A mask, region of interest (ROI), was created for the cell membrane using thresholds recommended by the software. Similarly, a mask, ROI of the Hapln1-Myc protein was created using software recommended thresholds. All masks were validated by visualization ensuring no over or under saturation. Colocalization graphs were created by the software. Slides were imaged using Zeiss LSM880.

Cell membrane isolation

Cell membrane pull down was done on HEK 293T cells. Briefly, 250k HEK 293T cells were seeded in a 6 well plate. About 24 hours later cells were transfected with WT, C306S, or ET *Hapln1* plasmids as described in the Fractionation and Western blot Methods section. After 48 hours cells were rinsed twice with PBS followed by incubation with 0.5mg/mL EZ-Link Sulfo-NHS-SS-Biotin (Fisher Scientific, cat. no. PI21331) in PBS on ice for 1 hour. The reaction was quenched by washing the wells with 150mM glycine in TBS. The cells were lysed by

adding RIPA buffer (Fisher Scientific, cat. no. PI89900) with Halt Protease Inhibitor cocktail (Fisher Scientific, cat. no. PI87786), on ice for 30 minutes. The cell lysate was then spun down at 12,000 rpm for 10 minutes at 4°C and the supernatant (cell lysate) was saved. The cell lysate was added to Pierce Streptavidin Agarose (Fisher Scientific, cat. no. PI20349). The agarose beads were washed in PBS and membranes were eluted in Pierce IgG Elution Buffer (Fisher Scientific, cat. no. PI21004). The membrane proteins pulled down were further analyzed on a Western blot as described in the Fractionation and Western blot Methods section.

CHAPTER FOUR

Results

JIA – WISP3 study. Please see Appendix 1.

AIS – GWAS study. Please see Appendix 2.

Identifying new high-risk loci.

To identify new high-risk loci, we analyzed WGS on 72 families with co-segregating, dominantly inherited AIS. In this study we limited our search space to rare nonsynonymous variants (MAF <1%) in the Genome Aggregation Database (gnomAD). The list of candidate variants was further filtered for those genes appearing in at least two independent families, with prioritization of those genes having a published role in cartilage development (Figure 2C). From this analysis we identified the gene *HAPLN1*, Hyaluronan And Proteoglycan Link Protein 1, also known as *CRTL1*, Cartilage Link Protein 1. Multiple *HAPLN1* mutations were discovered in the GMKF cohort, with predicted protein mutations as shown in Table 2. Additional mutations were found in a separate cohort (N=369) through whole exome sequencing (WES) screening of affected individuals, and family members when available. Of the seven protein-altering variants, we noted that four occurred within the B' domain of the protein (Figure 2B). Of those four, C304S, G336S, and P317A, were considered for further study (Figure 2D). The C304 residue in *HAPLN1* is one of five “critical” disulfide-bonded cysteines in the B' link module as demonstrated by reported solution structure (Blundell et al., 2005; Roughley, 2006). Molecular modeling of the C304S mutated protein, based off the

solved link module structure (Blundell et al., 2005), predicted disruption of the B' link module and potential interference with HA binding (Figure 3).

CHR 5 BP	RsID	NM_001884Change	AChange	gnomAD_NFE	CADD/GERP
82937374	rs148624914	exon5:c.G1006A	G336S	0.0006	24.1/5.22
82937469	rs747962449	exon5:c.G911C	C304S	.	16.74/4.33
82937431	.	exon5:c.C949G	P317A	.	24.7/5.22
82937538	rs6864342	exon5:c.A842G	N281S	0.0069	0.001/1.34
82940451	rs374286486	exon4:c.G506A	R169H	0.00001274	35/5.8
82948541	.	exon3:c.C203G	T68R	.	14.67/5.18
82948425	rs139457628	exon3:c.G319A	G107S	0.00001	7.13/-0.79

Table 2. HAPLN1 mutations identified in WGS and WES screen. cDNA mutations of two variants found through WGS are shown in bold. Five additional variants found through WES are shown with their corresponding amino acid change. * G336S was found in both WGS and WES screens.

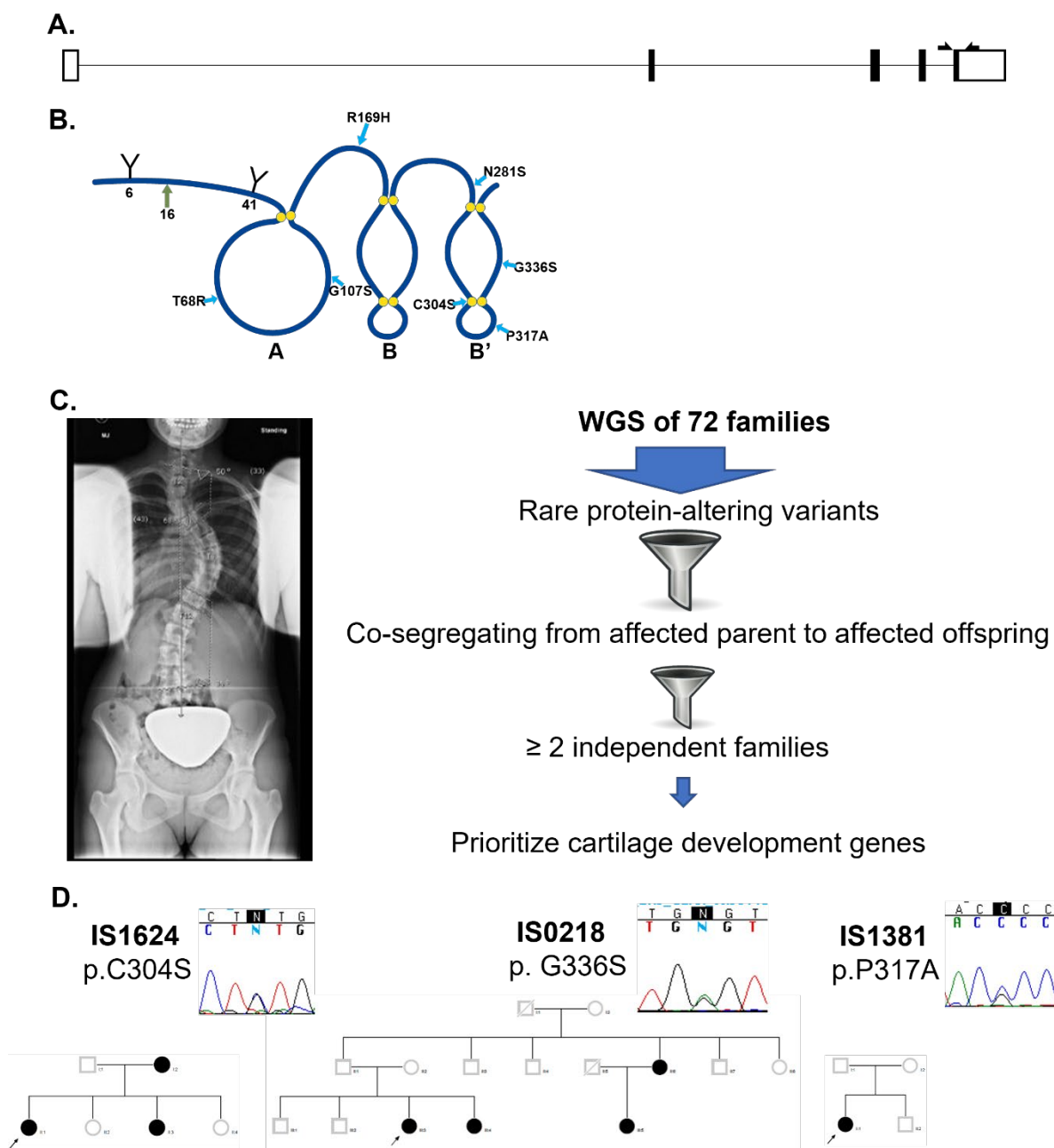


Figure 2. Genome sequencing strategy to identify candidate variants in subjects with AIS. A. Cartoon depicting the five exons of *HAPLN1*. White boxes indicate UTR, lines indicate introns, and arrows indicate genotyping primers. **B.** Cartoon showing the three domains of *HAPLN1* with AIS-co-segregating mutations. The *HAPLN1* protein can be found with one or two oligosaccharides attached on the 6th and 41st residues. A N-link peptide is also found by cleavage after the 16th residue. **C.** 13-year-old female with AIS, before surgical correction. WGS of 287 individuals from 72 families with dominantly inherited AIS was performed. Nonsynonymous (i.e., protein-altering) variants with minor allele frequency (MAF) $\leq 1\%$ in the Genome Aggregation Database (gnomAD) were filtered, with

further prioritization of those variants that co-segregated with AIS, in genes with a biologic role in cartilage development and identified in at least 2 independent families. **D.** Sanger sequencing of the proband with HAPLN1 mutations: IS1624 (C304S), IS0218 (G336S), and IS1381 (P317A).

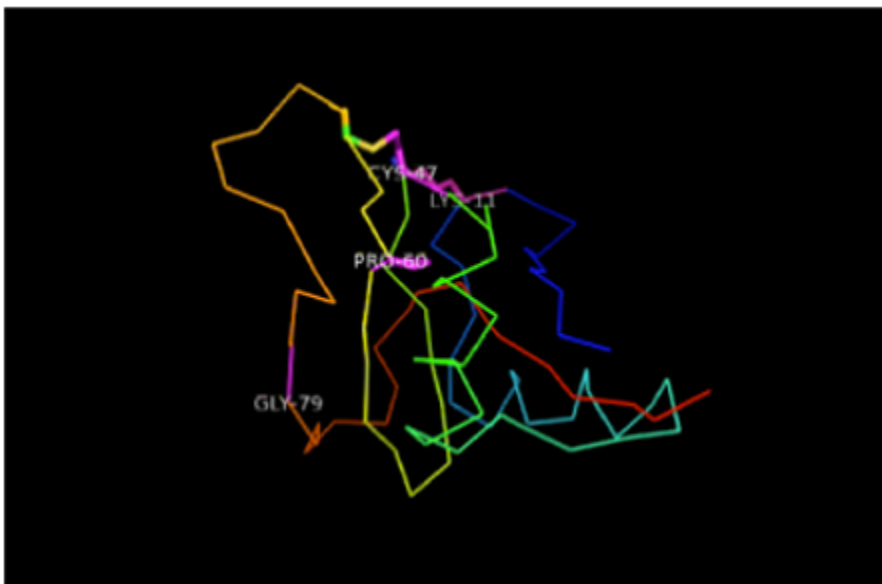


Figure 3. Molecular modeling of the C304S (Cys-47) mutated protein. Molecular modeling based off the solved single link module indicates that the novel mutation, C304S, predicted to disrupt the hydrophobic core of the protein. Modeling performed courtesy of Dr. Jimin Pei and Dr. Nick Grishin.

C306S (human C304S) mutation in Hapln1 impairs its retention in the ECM in vivo.

To investigate the human mutations found through the WGS screen, I created the orthologous mouse mutations by mutagenesis in a commercially available mouse *Hapln1* expression vector containing a c-terminal Myc-tag (Origene, Cat. no. MR205436) (Figure 4A). Additionally, I also created a truncated construct lacking the c-terminal loop domain C306Sfs*5 (ET). I then transfected these constructs into COS-7 cells and monitored the expressed protein with anti-Myc antibody detected by immunofluorescence microscopy. In this study, I found that Hapln1^{C306S} and Hapln1^{ET} proteins localized within the cell but not in the ECM space. However, WT, Hapln1^{G338S}, and Hapln1^{P319A} proteins were all detected both within the cell as

well as the ECM space (Figure 4B). To determine whether *Hapln1*^{C306S} or *Hapln1*^{ET} mutations were secreted into the media, I transfected HEK 293T cells and isolated the cell lysate, media, and ECM fractions. By Western blotting the cell lysate, media, and ECM fractions using anti-Myc antibody for detection, I found WT, *Hapln1*^{G338S}, and *Hapln1*^{P319A} proteins present in all three fractions. However, the *Hapln1*^{C306S} was only detected in the cell lysate and media fractions, while the *Hapln1*^{ET} protein was only detected in the cell lysate fraction (Figure 4C). Western blot was further probed for Gapdh which was not detected in the media and ECM fractions, indicating the signal was unlikely to be carryover from the cell lysate fraction where Gapdh was detected. Western blot further showed no distinct proteolytic processing of *Hapln1* in the transient transfection conditions. These results indicate that the *Hapln1*^{C306S} mutant protein is secreted into the media but not appreciably retained in the ECM, while the *Hapln1*^{ET} mutant protein is retained in the cells and not secreted *in vitro*.

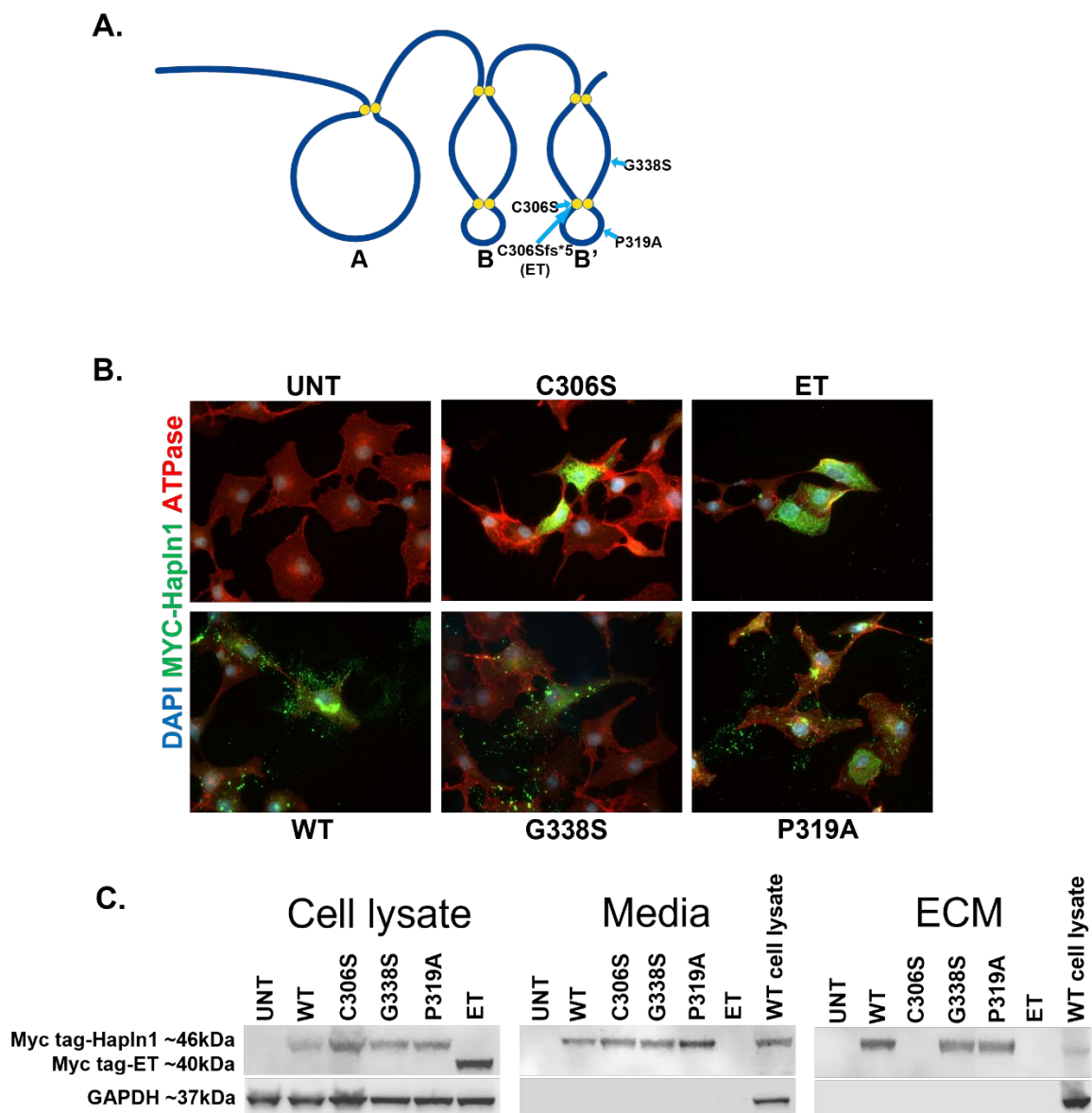


Figure 4. C306S (human C304S) mutation in Hapln1 impairs its retention in the ECM. **A.** Cartoon depicting the location of mutation of interest, C306S (human C304S), G338S (human G336S), P319A (human P317A), or a truncated protein lacking the C-terminal loop domain (“ET”, *Hapln1*C306fs*5). **B.** IF of mouse C-terminal myc-tagged Hapln1 constructs, overexpressed in COS-7 cells and detected with anti-myc antibody (green). Cell membrane was visualized using ATPase antibody (red). **C.** Western blot showing the cell lysate, media, and ECM of HEK 293T cells transfected with mouse WT, C306S, G338S, P319A, or ET. Hapln1 detected at ~46kDa, ET protein detected ~40kDa and Gapdh at ~37kDa. UNT=un-transfected control. GAPDH as loading control.

Cysteines are critical for the ECM retention of the Hapln1 protein.

To determine if other cysteines within the B and B' loops also play a role in the secretion of Hapln1, I individually mutated cysteines within the two loops to serines (Figure 5A). I transfected the Cys-Ser constructs into HEK 293T cells, and analyzed the cell lysate, media, and ECM fractions by Western blot. Western blotting revealed that mutating any of the cysteine residues 1, 4, 1', or 4' in the "backbone" of the B or B' loops caused Hapln1-Myc to be retained within the cell. When the cysteines 2, 3, 2', or 3' were mutated, the protein still retained the ability to be secreted into the media (Figure 5B). However, none of the eight mutant proteins were detected in the ECM fraction. These results support a model in which all disulfide bridges are required to be intact for the Hapln1 protein to be retained in the ECM, as detected by our methods.

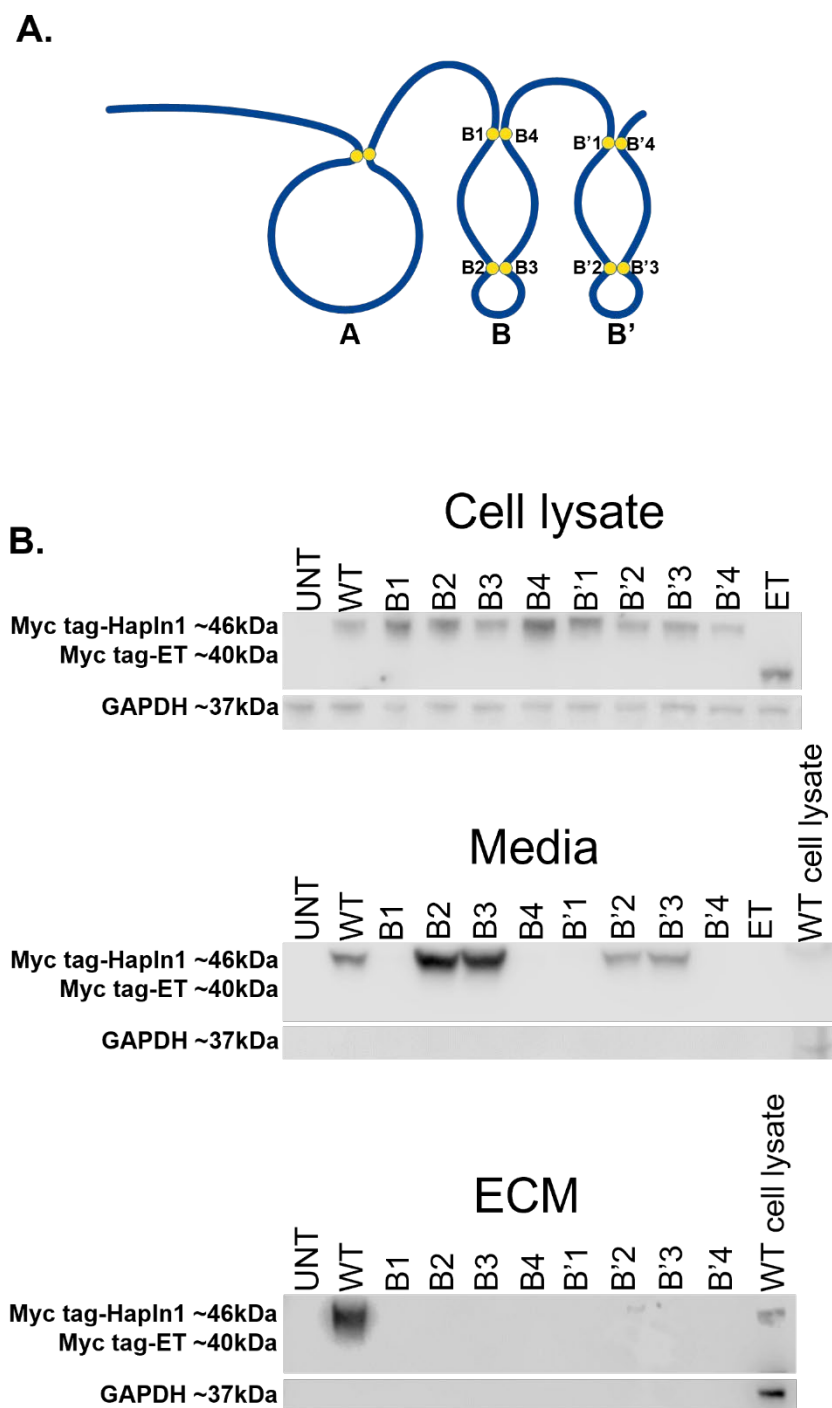


Figure 5. Disulfide bridges are critical for ECM retention of Hapln1 protein. **A.** Cartoon depicting the Cys-Cys disulfide bridges in the Hapln1 protein. Each cysteine was individually mutated to serine in experiments shown in (B). **B.** Western blot of HEK 293T cells transfected with mouse WT, and individually mutated Cys to Ser residues in the B and B' loops as denoted in A, detected with anti-myc

antibody. Hapln1 detected at ~46kDa, ET protein detected ~40kDa and Gapdh at ~37kDa. UNT=un-transfected control.

No colocalization between the Hapln1 protein and the cell membrane.

To determine if the Hapln1^{C306S} or Hapln1^{ET} mutations were instead adhering to the cell membrane, I performed a cell membrane pull down. I transfected HEK 293T cells with WT, Hapln1^{C306S} or Hapln1^{ET} mutant plasmid followed by biotinylating the cell membrane and performing a pull-down using Streptavidin conjugated agarose beads. The pull-down cell membrane fractions were then analyzed by Western blot. Neither the WT, Hapln1^{C306S} or Hapln1^{ET} proteins were detected on the cell membrane fraction, but were readily detected in the unbound fraction, that the transfection worked. (Figure 6A). To confirm these results, I collected IF z-stack images of COS-7 cells transfected with WT, Hapln1^{C306S} or Hapln1^{ET} plasmids. Cell membrane was stained using anti-ATPase, and Hapln1 was detected using anti-Myc. To test colocalization I created a region of interest (ROI) around the cell membrane and analyzed any colocalization with the Hapln1 protein, using Imaris x64 version 9.5.1 analysis software, UT Southwestern, Live Cell Imaging Core. These analyses further validated no correlation between the cell membrane and the WT, Hapln1^{C306S} or Hapln1^{ET} proteins, by IF (Figure 6B). Thus, we conclude that the secreted Hapln1^{C306S} is not bound to the cell membrane.

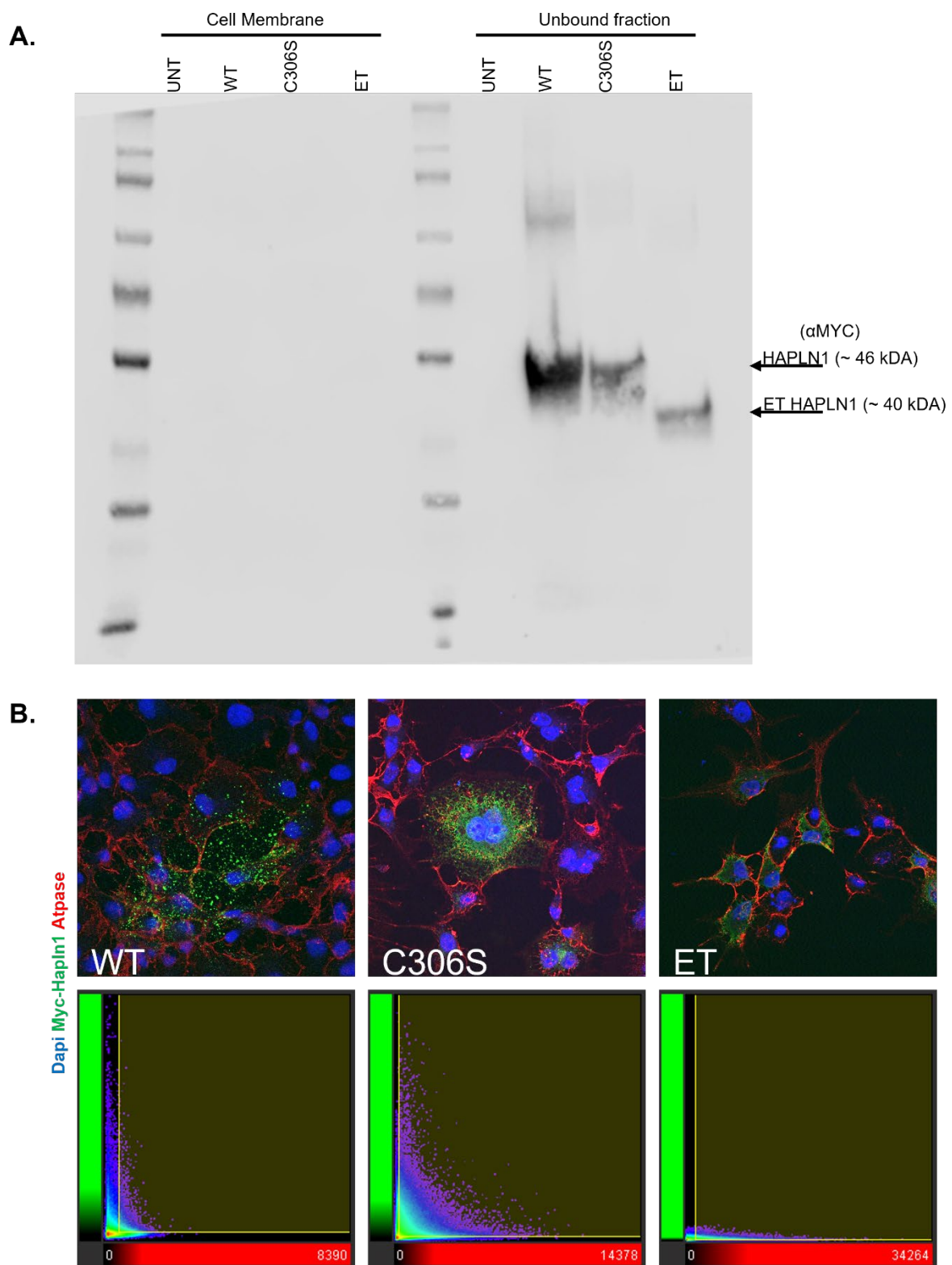


Figure 6. Pull-down of biotinylated membrane proteins show no co-localization of Hapln1

protein on the cell membrane. A. Western blot of the cell membrane pull-down and unbound fraction cell lysate as a positive control. **B.** Maximum intensity projection (MIP) images of COS-7 cells transfected with WT, C306S, or ET. detected with anti-myc antibody (green). Cell membrane was visualized using ATPase antibody (red). UNT=un-transfected control.

Hapln1^{C306S/C306S} mice appear normal, while Hapln1^{ET/ET} mice display classic chondrodysplasia.

To evaluate the consequences of the C306S and ET mutation *in vivo*, mice were engineered harboring the *Hapln1^{C306S}* or *Hapln1^{ET}* alleles using CRISPR/Cas9 gene editing by the UT Southwestern Transgenic Core facility, Dr. Robert Hammer, Director (Figure 7A). Homozygous *Hapln1^{ET/ET}* mice died shortly after birth, showing dwarfism with chondrodysplastic phenotype, similar to previously reported knock-out mice. However, homozygous *Hapln1^{C306S/C306S}* mice were viable and show no obvious differences from WT littermates (H. Watanabe & Yamada, 1999). To examine the skeletal structure in more detail, I performed whole-mount skeletal staining of WT, *Hapln1^{ET/ET}*, and *Hapln1^{C306S/C306S}*, of P0.5-day old mice. The whole-mount skeletal staining showed *Hapln1^{C306S/C306S}* mice with no obvious gross developmental abnormalities, with *Hapln1^{ET/ET}* mice showing bones of both the limbs and legs to be shorter and curved, with dome shaped skull, and smaller sphenoid and occipital bone (Figure 7B-C). To examine gross organ morphology, I performed H&E staining of whole mount sections of WT, *Hapln1^{ET/ET}*, and *Hapln1^{C306S/C306S}*, of P0.5 day old mice (Figure 8A). In cartilage (IVD and femoral growth plates) H&E staining of the IVD (Figure 8B), and cartilage of the femur (Figure 8C) I observed no obvious differences between WT and *Hapln1^{C306S/C306S}*. *Hapln1^{ET/ET}* mice, however showed highly disorganized IVD, with the nucleus pulposus appearing smaller, the annulus fibrosus appearing less tightly packed, the

endplate showing less chondrocytes, with the vertebral bodies looking smaller. Chondrocytes in femoral growth plate were likewise highly disorganized, particularly in the pre-hypertrophic and hypertrophic zones. *Hapln1* has been shown to be present in the heart, lungs, and brain, we are currently assessing morphology of these organs in more detail. Furthermore, homozygous *Hapln1*^{C306S/C306S} mice displayed no obvious skeletal abnormalities up to one year of age.

A.

		C306S		gRNA		R325R	
WT	GAAA...42bp...CGCT	TGC	GAT...27bp...CGCTATCCTATTTCTCGACCAAGA	AGG	CGC...42bp...GATAA		
C306S	GAAA...42bp...CGCT	TCC	GAT...27bp...CGCTATCCTATTTCTCGACCAAGA	AGA	CGC...42bp...GATAA		
C306fs*5	GAAA...42bp...CGCT	-C	GAT...27bp...CGCTATCCTATTTCTCGACCAAGA	AGA	CGC...42bp...GATAA		

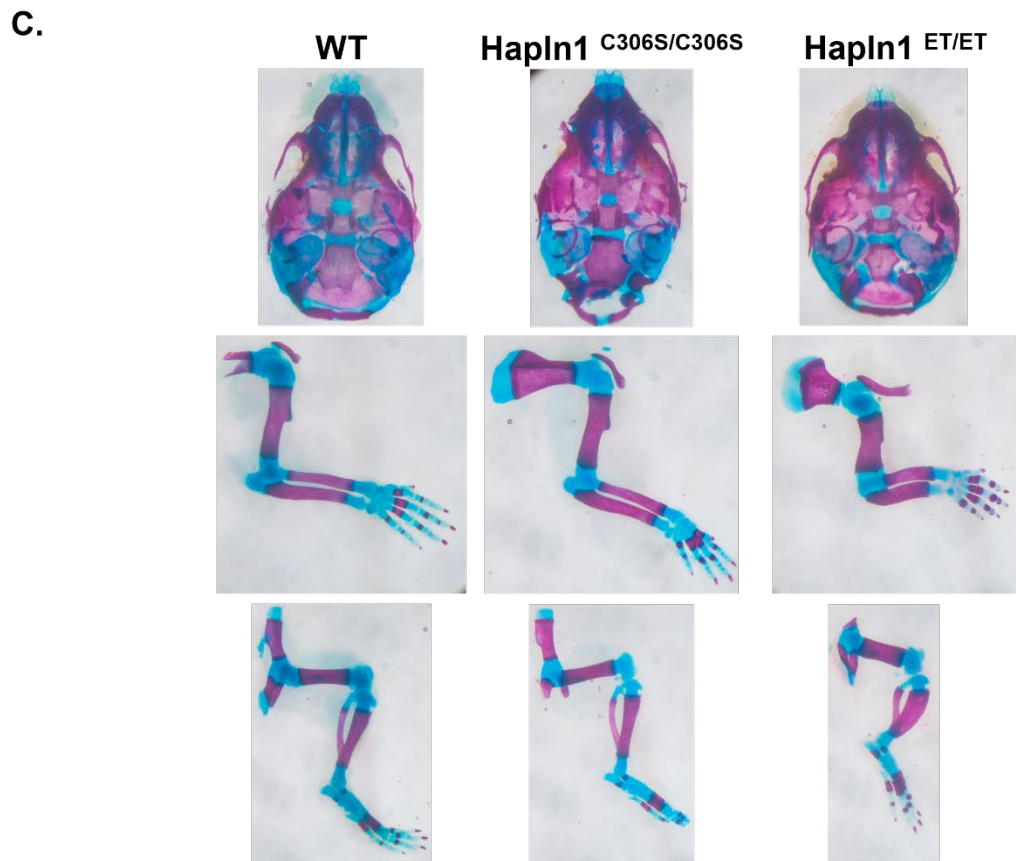
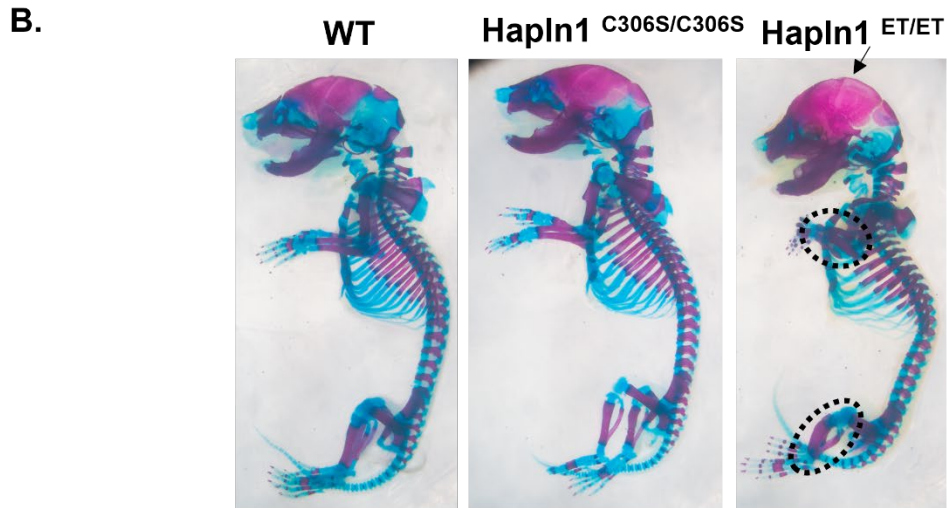


Figure 7. *Hapln1*^{C306S/C306S} and *Hapln1*^{ET/ET} mutant lines generated via CRISPR show chondrodysplastic phenotype in *Hapln1*^{ET/ET} mice. **A.** *Hapln1* mouse lines harboring C306S, and ET were generated by CRISPR. Displayed is the donor sequence used with the targeted site of mutation highlighted yellow, gRNA in blue with PAM site highlighted in purple. **B.** Skeleton preparations of P0.5-day old mice shown with Alizarin red-stained bones and Alcian blue-stained cartilage. Circle shows shortened limbs and arrow indicated dome-shaped head. **C.** Images of the skull, arm, and limb. Images shown are representative of at least N=3 animals.

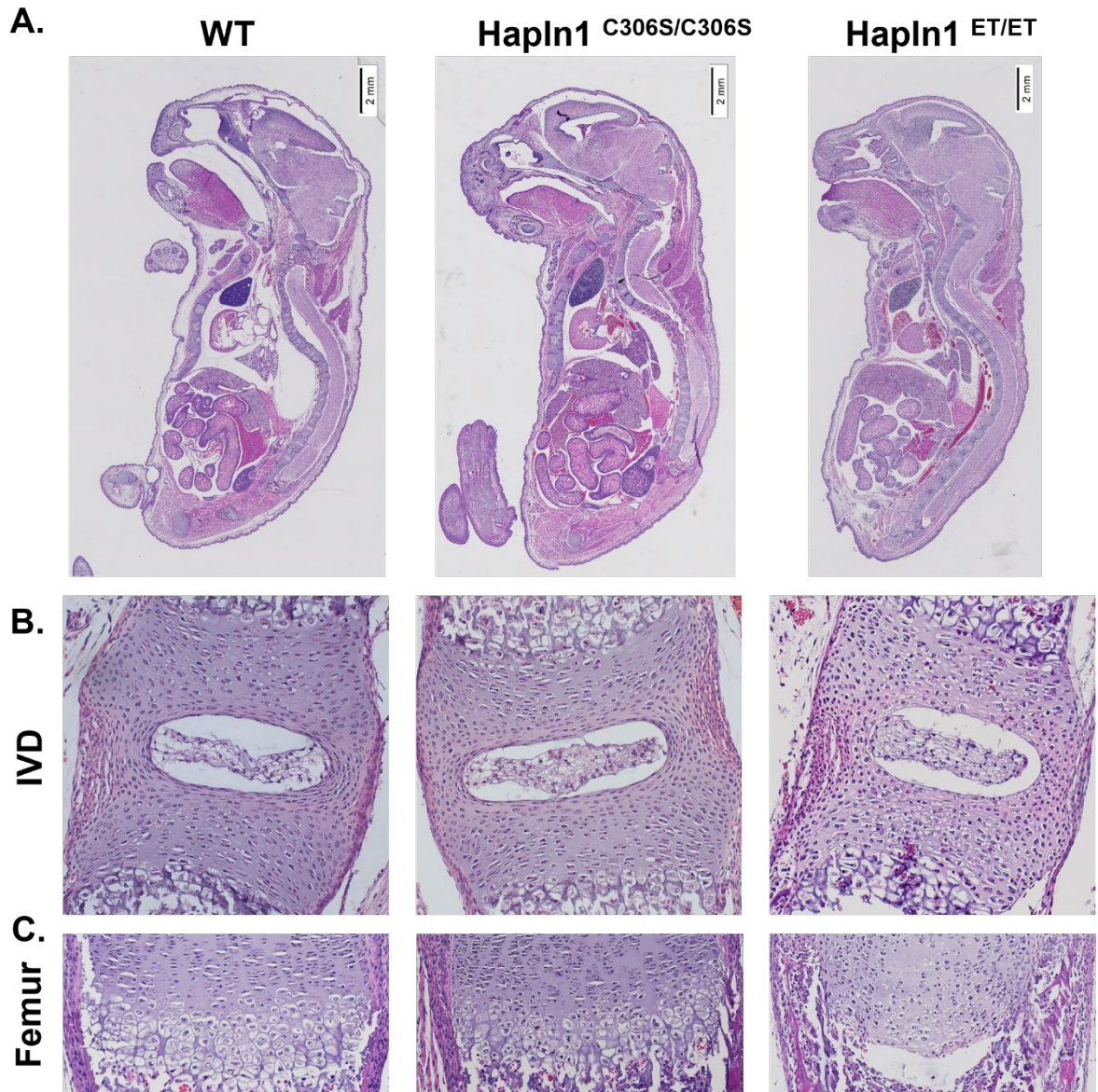


Figure 8. H&E of P0.5-day old *Hapln1*^{ET/ET} mice show complete disorganization of the IVD and femur. **A.** H&E of P0.5-day old WT, *Hapln1*^{C306S/C306S}, and *Hapln1*^{ET/ET} mice. **B.** H&E of the IVD **C.** H&E of the cartilage of the femur showing the pre-hypertrophic and hypertrophic zone.

Hapln1 protein is not detected in the growth plate of cartilage of *Hapln1*^{C306S/C306S} mutant mice.

To validate the Hapln1 antibody, I transfected HEK 293T cells with WT, *Hapln1*^{C306S}, or *Hapln1*^{ET} plasmids and analyzed using Western blot. The results confirmed the ability of the anti-Hapln1 antibody to be able to detect WT, Hapln1^{C306S}, and Hapln1^{ET} proteins by Western blot (Figure 9A). To determine if the anti-Hapln1 antibody could also detect the protein by IF, I transfected COS-7 with WT, *Hapln1*^{C306S}, or *Hapln1*^{ET} plasmids and analyzed for colocalization using IF, using the C-terminal Myc-tag and anti-Hapln1 antibody. The IF results further validated the anti-Hapln1 antibody by showing colocalization of the anti-Myc with anti-Hapln1 for the WT, Hapln1^{C306S}, and Hapln1^{ET} proteins (Figure 9B).

Using this validated antibody, I performed IHC staining for Hapln1 in the IVD and growth plate of the long bone in WT, *Hapln1*^{C306S/C306S}, and *Hapln1*^{ET/ET} P0.5-day old mice. In the WT animals, I saw the highest levels of Hapln1 signal in the endplate of the IVD and the hypertrophic zone in the femur. The IHC results showed a reduction in Hapln1 staining in heterozygous *Hapln1*^{C306S/+} and *Hapln1*^{ET/+} mice both in the growth plate of the long bone and IVD compared to WT (not shown). Furthermore, no signal was detected by IHC in homozygous *Hapln1*^{C306S/C306S} or *Hapln1*^{ET/ET} animals in either the IVD or long bone (Figure 10A-B). These results were replicated with IF (Figure 10C-D), where I detect Hapln1 specifically in the endplates of the IVD in WT mice, while no Hapln1 signal was detected in the growth plate in the bones of the *Hapln1*^{C306S/C306S} and *Hapln1*^{ET/ET} mice. However, I observed a faint Hapln1 signal in IVD regions of the spine of *Hapln1*^{C306S/C306S} mice, this could

be due to the higher sensitivity of IF, although bleed through from endogenous autofluorescence of the tissue could not be ruled out. This could potentially be real signal seen in the vertebral growth plate that is not seen in growth plate of the femur. We are currently looking into the differences between the growth plates of the vertebrae and the femur.

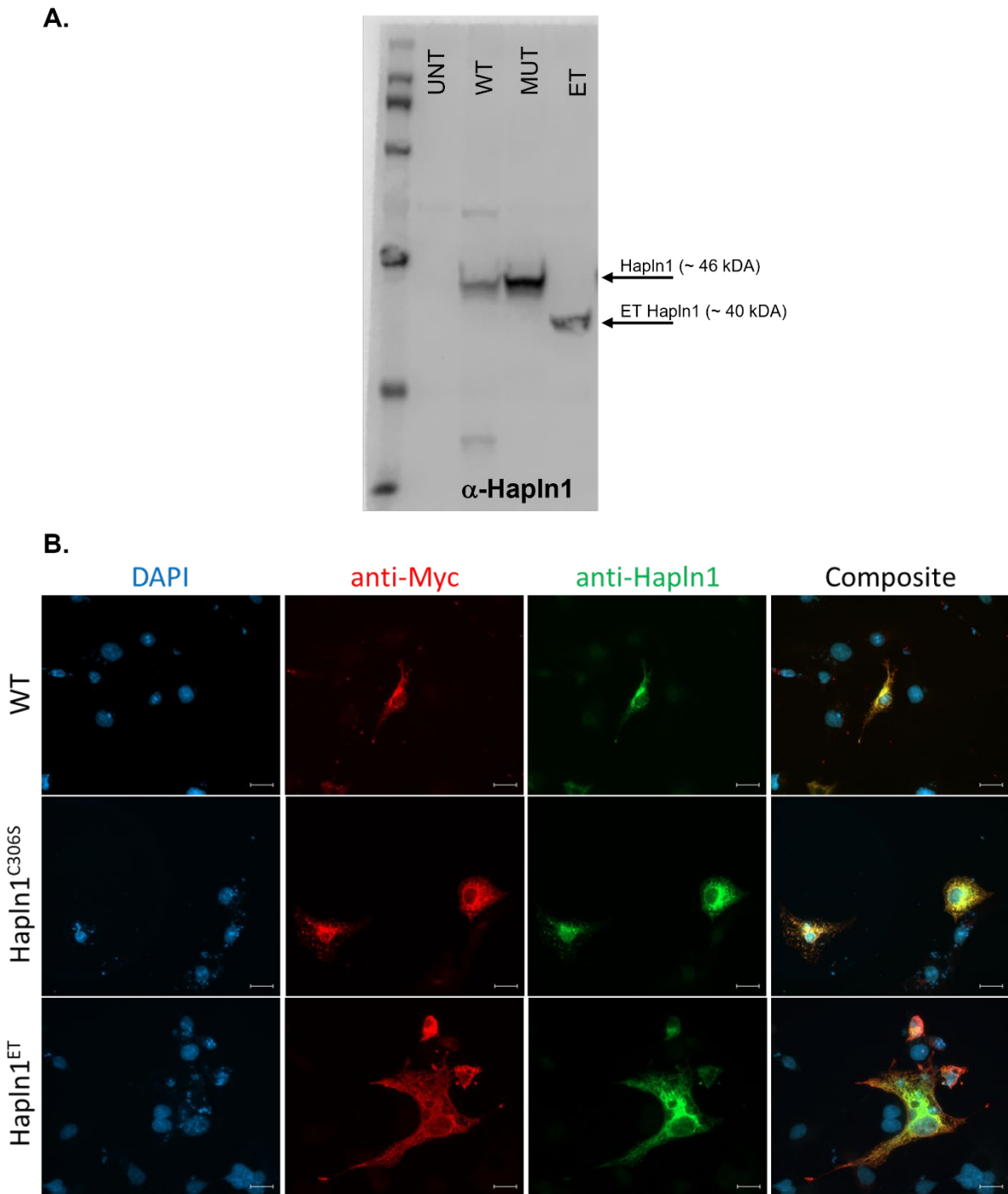


Figure 9. Validation of the monoclonal anti-Hapln1 antibody. **A.** Western blot of the cell lysate of HEK 293T cells transfected with the WT, C306S, and ET plasmid detected using anti-Hapln1. **B.** IF of COS-7 cells transfected with the WT, C306S, and ET plasmid detected using anti-Myc (red) and anti-Hapln1 (green). Nuclei are detected with DAPI (blue). UNT=un-transfected control.

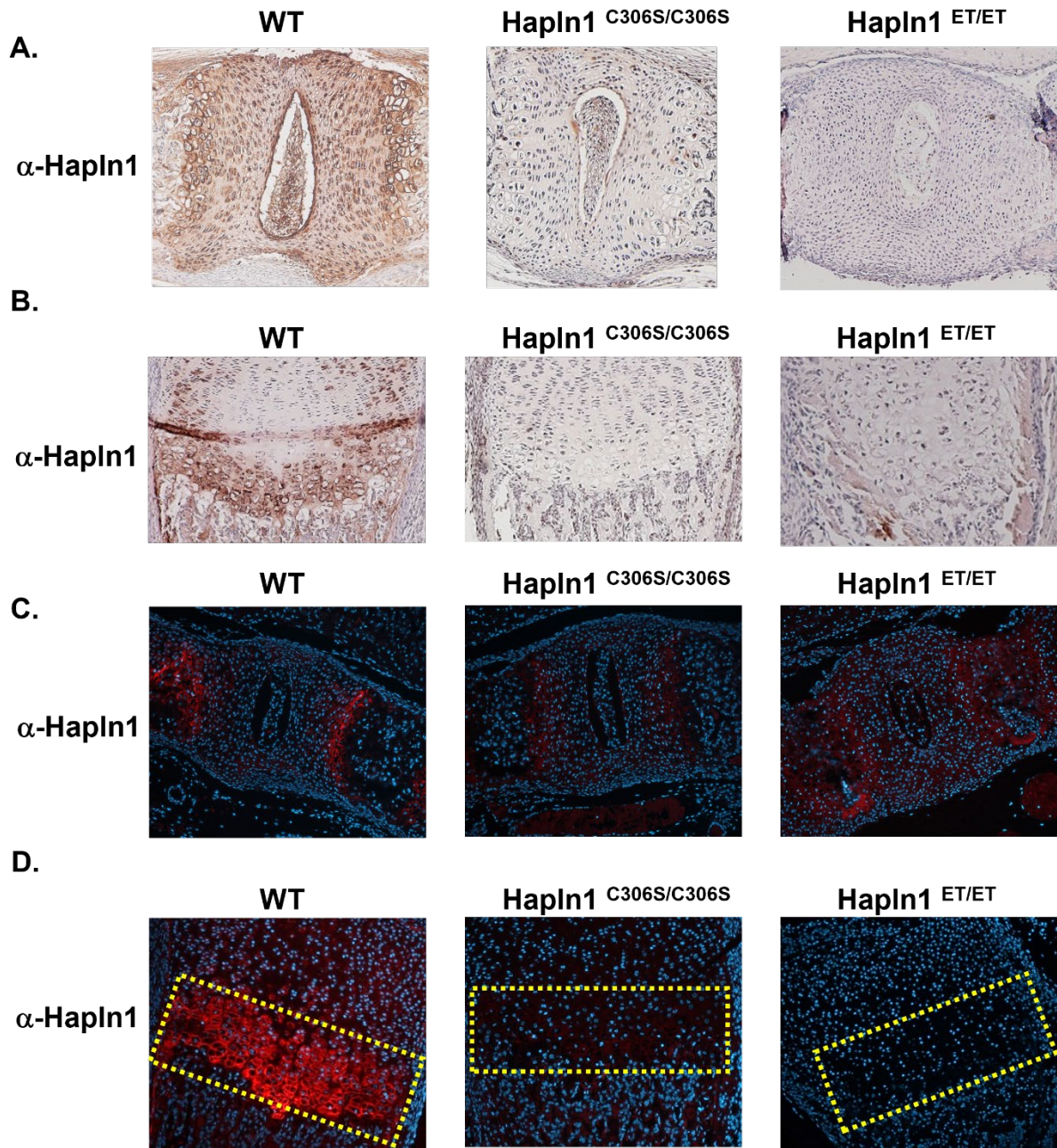


Figure 10. Hapln1 is undetected in *Hapln1*^{C306S/C306S} and *Hapln1*^{ET/ET} mice. IHC of P0.5-day old mice stained for anti-Hapln1 positive signal in brown and nucleus counterstained with hematoxylin in purple of **A.** IVD, and **B.** femur. IF staining with anti-Hapln1 in red and nucleus counterstained with DAPI in blue of **C.** IVD, and **D.** femur.

Hapln1 and *Coll10a1* mRNA are expressed in growth plates of P0.5-day old *Hapln1*^{C306S/C306S} mice, but greatly reduced in *Hapln1*^{ET/ET} mice.

Given the inability to detect the *Hapln1* protein in the growth plates of cartilage in *Hapln1*^{C306S/C306S} and *Hapln1*^{ET/ET} mutants, I elected to test its mRNA expression using RNAscope, UT Southwestern Metabolic Phenotyping core with the help of Dr. Laurent Gautron. When probed for *Hapln1* mRNA, both WT and *Hapln1*^{C306S/C306S} mice showed high expression in both the presumed pre-hypertrophic and hypertrophic zones, while *Hapln1*^{ET/ET} mice showed a severe reduction in signal in these regions compared to the WT and *Hapln1*^{C306S/C306S} (Figure 11A). Similarly, when probed for *Coll10a1* mRNA, a classical marker of the hypertrophic zone and growth plate (M. & V., 2014), both the WT and *Hapln1*^{C306S/C306S} mice showed uniform signal throughout the hypertrophic zone, while the *Hapln1*^{ET/ET} mice showed discontinuous sparse signal in a smaller region presumed to be the hypertrophic zone, which could not be precisely defined due to the severe disorganization of the zones within the cartilage in the *Hapln1*^{ET/ET} mice (Figure 11B). These results demonstrate that the *Hapln1*^{C306S/C306S} mice still express normal levels of *Hapln1* and *Coll10a1* mRNA during early postnatal development, and in the appropriate regions, while *Hapln1*^{ET/ET} mice show dramatically reduced expression of both the *Hapln1* and *Coll10a1* mRNA in the hypertrophic zone during early development. Furthermore, the growth plate in *Hapln1*^{ET/ET} was disorganized and showed a reduced number of cells making it harder to comment if *Hapln1* mRNA was detected throughout the entirety of the hypertrophic zone in these animals. I hypothesize that the reduction in *Hapln1* mRNA in *Hapln1*^{ET/ET} mice is due to nonsense-mediated RNA decay.

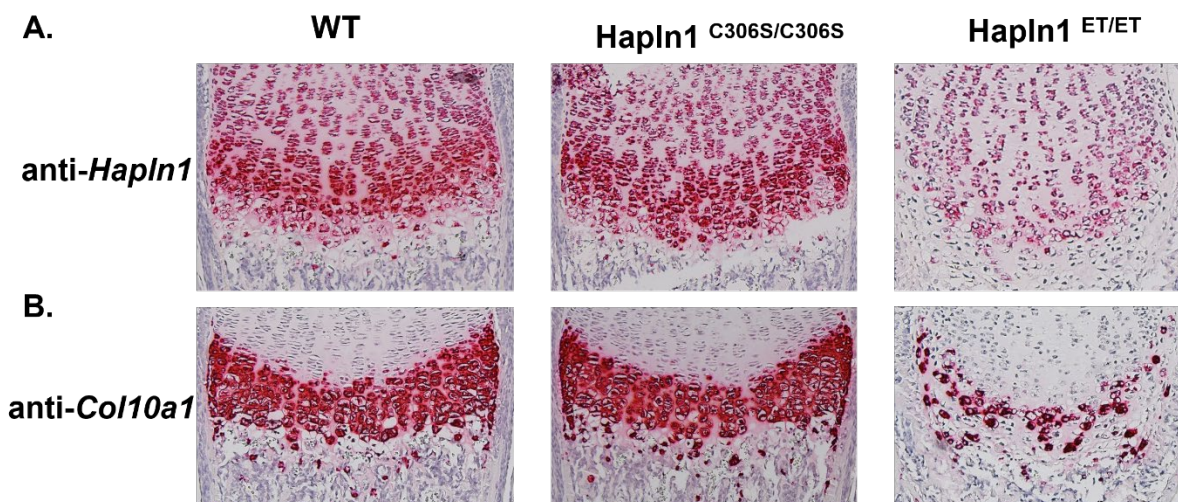


Figure 11. *Hapln1* and *Col10a1* mRNA is expressed in the growth plate of P0.5-day old *Hapln1*^{C306S/C306S} and WT mice while *Hapln1*^{ET/ET} mice show reduction in their levels. A. RNA scope of *Hapln1* mRNA targeting the 5' region upstream of the mutations shows WT like expression pattern in *Hapln1*^{C306S/C306S} mice but reduced signal in *Hapln1*^{ET/ET} mice. **B.** Consecutive slides were stained for *Col10a1* mRNA showing no differences between WT and *Hapln1*^{C306S/C306S} mice, while *Hapln1*^{ET/ET} mice showed nonuniform signal with reduction in the total number of cells positive for *Col10a1* in the hypertrophic zone. Chromogenic signal in red with nuclei counterstained with hematoxylin.

Hapln1^{ET/ET} mice have reduced proteoglycans and disorganized ECM.

Total proteoglycan levels were assessed in the growth plates of all three genotypes using Safranin O staining, performed in the Scottish Rite for Children histology core by Reuel Cornelia. Safranin O is a basic dye that stains negatively charged glycosaminoglycan chains, where the intensity of the staining is directly proportional to the proteoglycan content in the cartilage (Rosenberg, 2013). Surprisingly, although we could not detect *Hapln1* expression in the cartilage of *Hapln1*^{C306S/C306S} mice, proteoglycan staining of the growth plates of *Hapln1*^{C306S/C306S} mice appeared normal, identical to WT littermates. In contrast, Safranin O staining revealed a dramatic reduction in staining for total proteoglycan levels in *Hapln1*^{ET/ET} mice compared to WT and *Hapln1*^{C306S/C306S} mice (Figure 12A). Furthermore, staining was

even reduced in the bone matrix of the *Hapln1*^{ET/ET} mice while WT and *Hapln1*^{C306S/C306S} mice showed no obvious differences. I next performed IF staining for individual ECM proteins Aggrecan and Type X Collagen, Col10a1. Staining for Aggrecan, an ECM protein and Hapln1 binding partner in cartilage, showed positive staining in the pre-hypertrophic and hypertrophic zones in WT and *Hapln1*^{C306S/C306S} mice. Aggrecan in *Hapln1*^{ET/ET} mice, however, showed a diffuse signal in the pre-hypertrophic and hypertrophic zones compared to WT and *Hapln1*^{C306S/C306S} mice which displayed a more distinct signal predominately surrounding the cells (Figure 12B). Similarly, Col10a1 staining was also strongest surrounding cells within the hypertrophic zone of WT and *Hapln1*^{C306S/C306S} mice. However, Col10a1 staining in *Hapln1*^{ET/ET} mice showed a diffuse staining throughout the entirety of the cartilage (Figure 12C) in contrast to mRNA expression in only a few cells as detected by RNAscope (Figure 11B). These results conclusively show a disruption of the ECM in *Hapln1*^{ET/ET} mice as seen by a reduction in total proteoglycan staining. Additionally, IF of the ECM proteins Aggrecan and Col10a1 suggest less tightly pack protein as seen by a more diffuse signal in *Hapln1*^{ET/ET} mice. Furthermore, these results show that while Hapln1 was undetected (Figure 12D) in *Hapln1*^{C306S/C306S} mice, the ECM space is indistinguishable from WT.

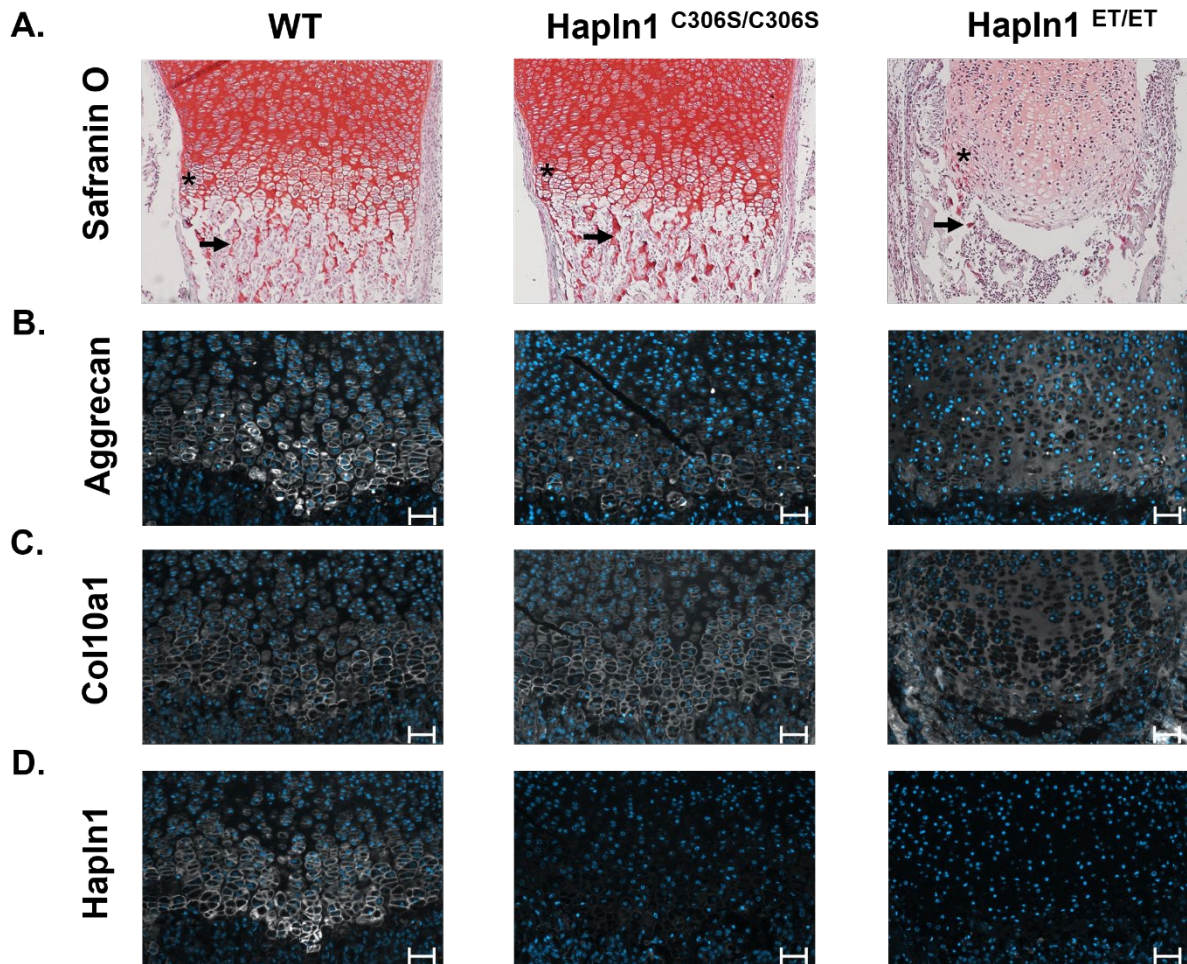


Figure 12. The growth plate of *Hapln1*^{ET/ET} mice shows reduction in total proteoglycan levels, Aggrecan, and Collagen X compared to WT and *Hapln1*^{C306S/C306S} mice. A. Safranin O/fast green staining of femurs of P0.5-day old pups with the nucleus counterstained with hematoxylin. Cartilage tissue, extracellular matrix, and muscle are stained red, collagen and cytoplasm are stained gray green, and nucleus are stained black. **B.** IF staining of Aggrecan **C.** Col10a1, and **D.** Hapln1. Arrows pointing to bone matrix, and * indicating the hypertrophic zone. Positive IF staining in white. Nuclei stained with DAPI in blue. 50um scale bar.

Apoptotic cells are increased in Hapln1^{ET/ET} mice compared to *Hapln1*^{C306S/C306S} and WT mice.

Our histological and immunofluorescence analyses of the growth plate sections of *Hapln1* mutant mice suggested that loss of intact Hapln1 in the *Hapln1*^{ET/ET} mutants leads to loss of

cells in the hypertrophic zone. To test if this could be due to increased apoptosis, Terminal Deoxynucleotidyl Transferase (TdT)-Mediated dUTP Nick-End Labeling (TUNEL) assays were performed, UT Southwestern, Histopathology core. In this method, blunt ends of double-stranded DNA, an established marker of apoptotic cells, are detected and quantified by catalytically attaching a fluorescein-12-dUTP at the 3'-OH end of the blunt end of fragmented DNA using Terminal Deoxynucleotidyl Transferase (TdT). Positive apoptotic signal is detected by the presence of fluorescein with the nuclei counterstained with propidium iodide. The TUNEL assay showed a dramatic increase in cells positive for apoptosis within the hypertrophic zone in the *Hapln1*^{ET/ET} mice, while WT and *Hapln1*^{C306S/C306S} mice showed minimal number of apoptotic cells (Figure 13). These results indicate that, in the absence of intact Hapln1, apoptosis is upregulated in cells within the hypertrophic zone of the growth plate. These results would explain the decrease in cell density in *Hapln1*^{ET/ET} mice along with a decrease in the number of cells positive for *Coll10a1* mRNA in this region.

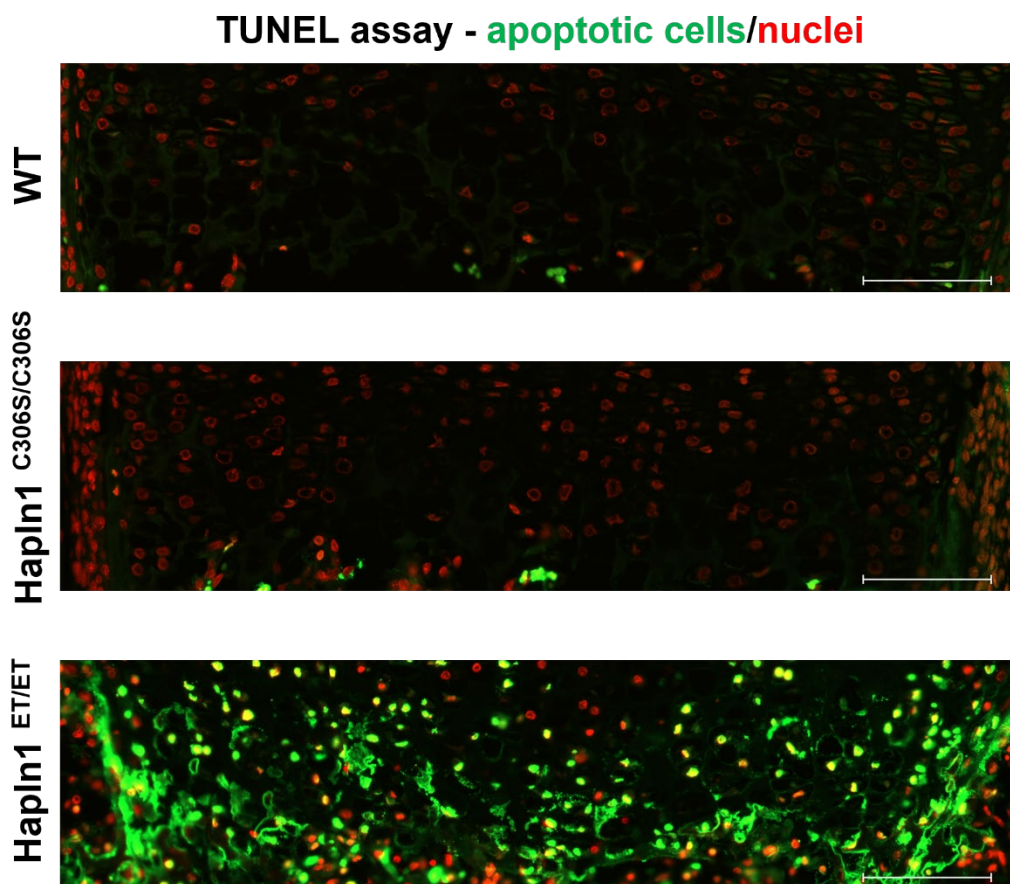


Figure 13. The growth plate of *Hapln1*^{ET/ET} mice shows an increase in cells positive for apoptosis compared to WT and *Hapln1*^{C306S/C306S} mice. TUNEL assay showed a higher number of cells positive in the hypertrophic zone of *Hapln1*^{ET/ET} mice compared to WT and *Hapln1*^{C306S/C306S} mice. Fluorometric TUNEL System was used to detect apoptosis with positive signal in green and nucleus counterstained in red. 100um scale bar.

μCT shows increased porosity in *Hapln1*^{ET/ET} cortical bone.

To study the extent of chondrodysplasia and bone defect in *Hapln1*^{ET/ET} mice micro-computed tomography (*μCT*) was performed by Dr. Aysha Khalid, a research scientist in our laboratory. *μCT* was performed on p0.5-day old WT, and *Hapln1*^{ET/ET} pups with voxel size of 8μm. WT mice showed a solid cortical bone structure while *Hapln1*^{ET/ET} mice showed severe porosity in the cortical bone (Figure 14). We expect that *Hapln1*^{C306S/C306S} effects on bone porosity, if any,

will be subtle. μ CT studies to address this question in newborn and 6-month-old mice are in progress.

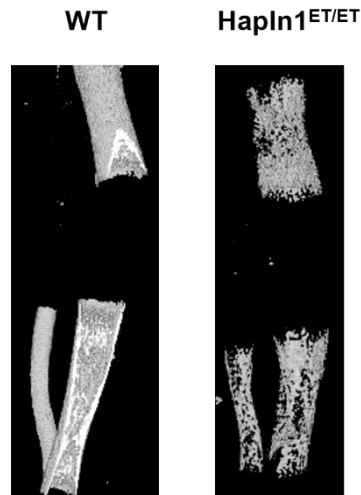


Figure 14. *Hapln1*^{ET/ET} mice show malformation of bone in p0.5 days old mice. μ CT, performed at 8 μ m resolution, show higher level of porosity in the cortical shell of *Hapln1*^{ET/ET} femur, tibia and fibula compared to WT mice.

CHAPTER FIVE

Conclusions and Recommendations

Using the sequence analysis pipeline established in our laboratory, and by applying biologic parameters, we identified AIS candidate genes for further analysis. From this pipeline I focused my attention on the *HAPLN1* gene. While multiple mutations were found within this gene, I decided to focus my attention on the C306S mutation, predicted to disturb a disulfide bridge that was thought to be critical to the function of this protein. My initial *in vitro* data showed that the C306S mutation still retains the ability to be secreted but lacks the ability to be retained in the ECM. To further support my findings, I mutated the connecting cysteine in this disulfide bridge, and the results mirrored my C306S findings. Further, I went on to test all disulfide bridges in both the B and B' loops. My results demonstrated that, *in vitro*, disruption of the primary disulfide bridges in the “backbone” of the protein hinders the protein’s ability to be secreted while deletion of the smaller inner disulfide bridges still allows the protein to be secreted but unable to attach to the ECM. I further showed that the “ET” mutant, C306S*fs5, lacking any disulfide bridges in the B' loop mimics the *in vitro* results seen by removing the “backbone” disulfide bridge of either loop, i.e., that it fails to be secreted from the cell. From these results, I hypothesize that homozygous mutations disrupting primary disulfide bridges will result in perinatal lethality, as observed with the ET mice (see below). Further work is needed to understand the kinetics of binding between HA or aggrecan and mutant forms of Hapln1.

Introduction of the ET mutation in mice resulted in perinatal lethality. Cause of lethality was not defined, but respiratory issues are suspected similar to that of a previously published KO (H. Watanabe & Yamada, 1999). Expression of *Hapln1* has been published in the heart, lungs, and brain, these organs need to be studied further to assess the full effect of *Hapln1* in early development. For the scope of this dissertation, I limited our assessment of *Hapln1* to the skeletal system. Skeletal evaluation of *Hapln1*^{ET/ET} mice showed severe developmental deformity, chondrodysplastic phenotype, that was consistent with published knockout (H. Watanabe & Yamada, 1999). As expected, no *Hapln1* protein was detected in these mice. Furthermore, little *Hapln1* mRNA was detected in these mice, possibly due to nonsense-mediated RNA decay. We expect that this line is a functional null. Spines of *Hapln1*^{ET/ET} mice showed severe disorganization of the IVD. Specifically, I observed that the annulus fibrosus appeared less tightly packed, the endplate showing fewer chondrocytes, and smaller nucleus pulposus. Additionally, vertebral bodies appeared smaller. In the long bones (femur) of *Hapln1*^{ET/ET} mice we observed highly disorganized growth plates. Normally, chondrocytes undergo differentiation starting from the epiphyseal side of the growth plate where they proliferate, become hypertrophic, and finally reach terminal differentiation where they undergo apoptosis. The hypertrophic chondrocytes in the growth plate are directly responsible for the longitudinal bone growth. Skeletal dysplasia has been widely noted when genes involved in the expression or regulation of the ECM of cartilage are disturbed (Alman, 2008). However, contrary to previously published data, our *Hapln1*^{ET/ET} mice showed an increase in cell apoptosis. My data further showed a reduced number of cells positive for the expression of *Col10a1* mRNA, a marker for the hypertrophic zone, the same area where high levels of

apoptosis was observed. These data support a model in which Hapln1 is a negative regulator of apoptosis in pre-hypertrophic/hypertrophic zones of the growth plate, directly or indirectly. Our characterization of the growth plates in these animals helps to explain the skeletal dysplasia we observed in the mice, i.e., the disorder in which the pre-hypertrophic and hypertrophic cells show disorganization, differential ECM production, and early apoptosis. Further work is warranted to understand the mechanism by which Hapln1 regulates apoptosis in the cartilaginous growth plate and potentially in other cell types.

Our analyses of *Hapln1*^{ET/ET} mice demonstrated that Hapln1 is essential for life. Furthermore, literature from the past ~40 years has pointed to Hapln1 as a critical player in ECM stability. Thus, the fact that we could not detect Hapln1 protein in our *Hapln1*^{C306S/C306S} mice, and yet they were viable and showed no obvious skeletal phenotype, was quite surprising. When probing for the presence of Hapln1 protein, results seemed to mimic results seen in the *Hapln1*^{ET/ET} mice. However, *Hapln1* and *Col10a1* mRNA both displayed expression similar to that of their WT littermates. When looking for apoptosis these animals showed minimal cell death, again mimicking WT. Probing for total proteoglycan levels, Aggrecan, and Col10a1 proteins, were all indistinguishable from WT. My *in vitro* results indicate that the C306S protein is properly secreted. Consistent with this, we have recently confirmed that we can detect appreciable levels of Hapln1 in plasma of human AIS patients (data not shown). I similarly hypothesize that the C306S protein is also being secreted *in vivo* and released into circulation. Additionally, a naturally occurring cleaved peptide of the N-terminus of HAPLN1 called “N-link” is proposed to upregulate the production of ECM genes by activation of BMP

receptor II. I suspect the secreted Hapln1^{C306S} protein continues to promote production of ECM genes. Further, I propose that this may be an essential role of Hapln1. In this model, the ECM would serve as a reservoir of Hapln1 protein that would be utilized during times of stress, e.g., rapid growth. While Hapln1 is known to facilitate the bind of proteoglycans to HA, it is not known if the Hapln1^{C306S} protein still possess this ability. It is possible Hapln1^{C306S} is still facilitating this binding yet due to its predicted change in protein structure it does not remain bound when the proteoglycan is added. It is also completely in the realm of possibility that in mice, Hapln1 is only needed in its secreted form to behave as a negative regulator of apoptosis.

The results from this study are worth studying further, in order to understand the roles that Hapln1 plays in early as well as later stages of development. Future directions from this study are to isolate chondrocytes from *Hapln1*^{ET/ET} mice to which media from cultured chondrocytes isolated from *Hapln1*^{C306S/C306S} mice or synthetic Hapln1^{C306S} protein would be added *in vitro* to test for upregulation of ECM genes. To test for apoptosis siRNA knockdown of *Hapln1* in cultured chondrocytes can be utilized to test for both upregulation of apoptosis and/or downregulation of proliferation. Furthermore, studies are needed to test for the presence of Hapln1 in circulation and whether that is altered for the Hapln1^{C306S} mutant and other mutants altering Hapln1 disulfide bridges. Finally, the kinetics and binding studies of Hapln1^{C306S} are needed to address if Hapln1^{C306S} still has the ability to bind HA sufficiently to be retained in the ECM.

APPENDIX A
JIA – WISP3 study

Patel C, Khanshour AM, Wilkes D, Rios JJ, Sheff KW, Nassi L, Wise CA. Novel homozygous variant in WISP3 in a family with unrecognized progressive pseudorheumatoid dysplasia. *Clin Case Rep.* 2020;8(8):1452-7. Epub 2020/09/05. doi: 10.1002/ccr3.2884. PubMed PMID: 32884773; PMCID: PMC7455413.

APPENDIX B
AIS – GWAS study

Khanshour AM, Kou I, Fan Y, Einarsdottir E, Makki N, Kidane YH, Kere J, Grauers A, Johnson TA, Paria N, Patel C, Singhania R, Kamiya N, Takeda K, Otomo N, Watanabe K, Luk KDK, Cheung KMC, Herring JA, Rios JJ, Ahituv N, Gerdhem P, Gurnett CA, Song YQ, Ikegawa S, Wise CA. Genome-wide meta-analysis and replication studies in multiple ethnicities identify novel adolescent idiopathic scoliosis susceptibility loci. *Hum Mol Genet.* 2018;27(22):3986-98. Epub 2018/11/06. doi: 10.1093/hmg/ddy306. PubMed PMID: 30395268; PMCID: PMC6488972.

BIBLIOGRAPHY

- Akbarnia, B. A. (2007). Management Themes in Early Onset Scoliosis. *The Journal of Bone & Joint Surgery*, 89(1), 42-54. doi:10.2106/JBJS.F.01256
- Al-Mayouf, S. M. (2018). Noninflammatory disorders mimic juvenile idiopathic arthritis. *Int J Pediatr Adolesc Med*, 5(1), 1-4. doi:10.1016/j.ijpam.2018.01.004
- Alman, B. A. (2008). Skeletal dysplasias and the growth plate. *Clin Genet*, 73(1), 24-30. doi:10.1111/j.1399-0004.2007.00933.x
- Antonarakis, S. E., Chakravarti, A., Cohen, J. C., & Hardy, J. (2010). Mendelian disorders and multifactorial traits: the big divide or one for all? *Nat Rev Genet*, 11(5), 380-384. doi:10.1038/nrg2793
- Asher, M. A., & Burton, D. C. (2006). Adolescent idiopathic scoliosis: natural history and long term treatment effects. *Scoliosis*, 1(1), 2. doi:10.1186/1748-7161-1-2
- Blundell, C. D., Almond, A., Mahoney, D. J., DeAngelis, P. L., Campbell, I. D., & Day, A. J. (2005). Towards a structure for a TSG-6-hyaluronan complex by modeling and NMR spectroscopy: insights into other members of the link module superfamily. *J Biol Chem*, 280(18), 18189-18201. doi:10.1074/jbc.M414343200
- Camenisch, T. D., Spicer, A. P., Brehm-Gibson, T., Biesterfeldt, J., Augustine, M. L., Calabro, A. J., . . . McDonald, J. A. (2000). Disruption of hyaluronan synthase-2 abrogates normal cardiac morphogenesis and hyaluronan-mediated transformation of epithelium to mesenchyme. *J Clin Invest*, 106(3), 349-360. doi:10.1172/JCI10272
- Carragee, E. J., & Lehman, R. A. J. (2013). Spinal bracing in adolescent idiopathic scoliosis. *N Engl J Med*, 369(16), 1558-1560. doi:10.1056/NEJMe1310746
- Chan, V., Fong, G. C., Luk, K. D., Yip, B., Lee, M. K., Wong, M. S., . . . Chan, T. K. (2002). A genetic locus for adolescent idiopathic scoliosis linked to chromosome 19p13.3. *Am J Hum Genet*, 71(2), 401-406. doi:10.1086/341607
- Czipri, M., Otto, J. M., Cs-Szabo, G., Kamath, R. V., Vermes, C., Firneisz, G., . . . Glant, T. T. (2003). Genetic rescue of chondrodysplasia and the perinatal lethal effect of cartilage link protein deficiency. *J Biol Chem*, 278(40), 39214-39223. doi:10.1074/jbc.M303329200
- Gao, X., Gordon, D., Zhang, D., Browne, R., Helms, C., Gillum, J., . . . Wise, C. (2007). CHD7 gene polymorphisms are associated with susceptibility to idiopathic scoliosis. *Am J Hum Genet*, 80(5), 957-965. doi:10.1086/513571

- Grover, J., & Roughley, P. J. (1994). The expression of functional link protein in a baculovirus system: analysis of mutants lacking the A, B and B' domains. *Biochem J*, *300* (Pt 2), 317-324. doi:10.1042/bj3000317
- Gruber, H. E., Hoelscher, G. L., Ingram, J. A., Bethea, S., Zinchenko, N., & Hanley, E. N., Jr. (2011). Variations in aggrecan localization and gene expression patterns characterize increasing stages of human intervertebral disk degeneration. *Exp Mol Pathol*, *91*(2), 534-539. doi:10.1016/j.yexmp.2011.06.001
- Haller, G., Alvarado, D., McCall, K., Yang, P., Cruchaga, C., Harms, M., . . . Gurnett, C. A. (2016). A polygenic burden of rare variants across extracellular matrix genes among individuals with adolescent idiopathic scoliosis. *Hum Mol Genet*, *25*(1), 202-209. doi:10.1093/hmg/ddv463
- Herring, J. A. (2008). *Tachdjian's pediatric orthopaedics*. Philadelphia, PA.
- Hresko, M. T. (2013). Clinical practice. Idiopathic scoliosis in adolescents. *N Engl J Med*, *368*(9), 834-841. doi:10.1056/NEJMcp1209063
- Karol, L. A., Johnston, C. E. n., Browne, R. H., & Madison, M. (1993). Progression of the curve in boys who have idiopathic scoliosis. *The Journal of Bone & Joint Surgery*, *75*(12), 1804-1810. doi:10.2106/00004623-199312000-00010
- Katz, D. E., Herring, J. A., Browne, R. H., Kelly, D. M., & Birch, J. G. (2010). Brace wear control of curve progression in adolescent idiopathic scoliosis. *J Bone Joint Surg Am*, *92*(6), 1343-1352. doi:10.2106/JBJS.I.01142
- Khanshour, A. M., Kou, I., Fan, Y., Einarsdottir, E., Makki, N., Kidane, Y. H., . . . Wise, C. A. (2018). Genome-wide meta-analysis and replication studies in multiple ethnicities identify novel adolescent idiopathic scoliosis susceptibility loci. *Human Molecular Genetics*, *27*(22), 3986-3998. doi:10.1093/hmg/ddy306
- Kim, K. H., & Kim, D. S. (2010). Juvenile idiopathic arthritis: Diagnosis and differential diagnosis. *Korean J Pediatr*, *53*(11), 931-935. doi:10.3345/kjp.2010.53.11.931
- Kiviranta, I., Jurvelin, J., Tammi, M., Säämänen, A. M., & Helminen, H. J. (1985). Microspectrophotometric quantitation of glycosaminoglycans in articular cartilage sections stained with Safranin O. *82*(3), 294-255. doi:10.1007/BF00501401
- Kornak, U., & Mundlos, S. (2003). Genetic disorders of the skeleton: a developmental approach. *Am J Hum Genet*, *73*(3), 447-474. doi:10.1086/377110

- Li, Y., Lacerda, D. A., Warman, M. L., Beier, D. R., Yoshioka, H., Ninomiya, Y., . . . Olsen, B. R. (1995). A Fibrillar Collagen Gene, Col1a1, Is Essential for Skeletal Morphogenesis. *Cell*, *80*(3), 423-430. doi:10.1016/0092-8674(95)90492-1
- Little, D. G., Song, K. M., Katz, D., & Herring, J. A. (2000). Relationship of peak height velocity to other maturity indicators in idiopathic scoliosis in girls. *The Journal of Bone & Joint Surgery*, *82*(5), 685-693. doi:10.2106/00004623-200005000-00009
- M., S. I., & V., R. M. (2014). *The Intervertebral Disc*: Springer Wien Heidelberg New York Dordrecht London.
- Mahoney, D. J., Blundell, C. D., & Day, A. J. (2001). Mapping the hyaluronan-binding site on the link module from human tumor necrosis factor-stimulated gene-6 by site-directed mutagenesis. *J Biol Chem*, *276*(25), 22764-22771. doi:10.1074/jbc.M100666200
- Martin, C. T., Pugely, A. J., Gao, Y., Mendoza-Lattes, S. A., Ilgenfritz, R. M., Callaghan, J. J., & Weinstein, S. L. (2014). Increasing hospital charges for adolescent idiopathic scoliosis in the United States. *Spine (Phila Pa 1976)*, *39*(20), 1676-1682. doi:10.1097/BRS.0000000000000501
- Murphy, R. F., & Mooney, J. F., 3rd. (2016). Complications following spine fusion for adolescent idiopathic scoliosis. *Curr Rev Musculoskelet Med*, *9*(4), 462-469. doi:10.1007/s12178-016-9372-5
- Nguyen, Q., Liu, J., Roughley, P. J., & Mort, J. S. (1991). Link protein as a monitor in situ of endogenous proteolysis in adult human articular cartilage. *Biochem J*, *278* (Pt 1), 143-147. doi:10.1042/bj2780143
- Ogura, Y., Takeda, K., Kou, I., Khanshour, A., Grauers, A., Zhou, H., . . . Ikegawa, S. (2018). An international meta-analysis confirms the association of BNC2 with adolescent idiopathic scoliosis. *Sci Rep*, *8*(1), 4730. doi:10.1038/s41598-018-22552-x
- Paria, N., Copley, L. A., Herring, J. A., Kim, H. K., Richards, B. S., Sucato, D. J., . . . Rios, J. J. (2013). Whole-exome sequencing: discovering genetic causes of orthopaedic disorders. *J Bone Joint Surg Am*, *95*(23), e1851-1858. doi:10.2106/JBJS.L.01620
- Rigueur, D., & Lyons, K. M. (2014). Whole-mount skeletal staining. *Methods Mol Biol*, *1130*, 113-121. doi:10.1007/978-1-62703-989-5_9
- Riseborough, E., & Wynne-Davies, R. (1973). A Genetic Survey of Idiopathic Scoliosis in Boston, Massachusetts. *The Journal of Bone & Joint Surgery*, *55*(5), 974-982.

- Rodriguez, E., & Roughley, P. (2006). Link protein can retard the degradation of hyaluronan in proteoglycan aggregates. *Osteoarthritis Cartilage*, *14*(8), 823-829. doi:10.1016/j.joca.2006.02.008
- Rogala, E. J., Drummond, D. S., & Gurr, J. (1978). Scoliosis: incidence and natural history. A prospective epidemiological study. *The Journal of Bone & Joint Surgery*, *60*(2), 173-176.
- Rosenberg, L. (2013). Chemical Basis for the Histological Use of Safranin O in the Study of Articular Cartilage. *The Journal of Bone & Joint Surgery*, *53*(1), 69-82.
- Roughley, P. J. (2006). The structure and function of cartilage proteoglycans. *Eur Cell Mater*, *12*, 92-101. doi:10.22203/ecm.v012a11
- Roughley, P. J., Lamplugh, L., Lee, E. R., Matsumoto, K., & Yamaguchi, Y. (2011). The role of hyaluronan produced by Has2 gene expression in development of the spine. *Spine (Phila Pa 1976)*, *36*(14), E914-920. doi:10.1097/BRS.0b013e3181f1e84f
- Salehi, L. B., Mangino, M., De Serio, S., De Cicco, D., Capon, F., Semprini, S., . . . Dallapiccola, B. (2002). Assignment of a locus for autosomal dominant idiopathic scoliosis (IS) to human chromosome 17p11. *Hum Genet*, *111*(4-5), 401-404. doi:10.1007/s00439-002-0785-4
- Sanders, J. O., Newton, P. O., Browne, R. H., Katz, D. E., Birch, J. G., & Herring, J. A. (2014). Bracing for idiopathic scoliosis: how many patients require treatment to prevent one surgery? *J Bone Joint Surg Am*, *96*(8), 649-653. doi:10.2106/JBJS.M.00290
- Sharma, S., Londono, D., Eckalbar, W. L., Gao, X., Zhang, D., Mauldin, K., . . . Wise, C. A. (2015). A PAX1 enhancer locus is associated with susceptibility to idiopathic scoliosis in females. *Nat Commun*, *6*, 6452. doi:10.1038/ncomms7452
- Spicer, A. P., Joo, A., & Bowling, R. A., Jr. (2003). A hyaluronan binding link protein gene family whose members are physically linked adjacent to chondroitin sulfate proteoglycan core protein genes: the missing links. *J Biol Chem*, *278*(23), 21083-21091. doi:10.1074/jbc.M213100200
- Tang, N. L., Yeung, H. Y., Hung, V. W., Di Liao, C., Lam, T. P., Yeung, H. M., . . . Cheng, J. C. (2012). Genetic epidemiology and heritability of AIS: A study of 415 Chinese female patients. *J Orthop Res*, *30*(9), 1464-1469. doi:10.1002/jor.22090

- Wang, Z., Weitzmann, M. N., Sangadala, S., Hutton, W. C., & Yoon, S. T. (2013). Link protein N-terminal peptide binds to bone morphogenetic protein (BMP) type II receptor and drives matrix protein expression in rabbit intervertebral disc cells. *J Biol Chem*, 288(39), 28243-28253. doi:10.1074/jbc.M113.451948
- Watanabe, H., Nakata, K., Kimata, K., Nakanishi, I., & Yamada, Y. (1997). Dwarfism and age-associated spinal degeneration of heterozygote *cmd* mice defective in aggrecan. *Proc. Natl. Acad. Sci. USA*, 94(13), 6943-6947. doi:10.1073/pnas.94.13.6943
- Watanabe, H., & Yamada, Y. (1999). Mice lacking link protein develop dwarfism and craniofacial abnormalities. *nature genetics*, 21(2), 225-229. doi:10.1038/6016
- Watanabe, H. Y., Yoshihiko. (2003). Chondrodysplasia of gene knockout mice for aggrecan and link protein. *Glycoconjugate Journal*, 19, 269-273.
- Weinstein, S. L., Dolan, L. A., Cheng, J. C. Y., Danielsson, A., & Morcuende, J. A. (2008). Adolescent idiopathic scoliosis. *The Lancet*, 371(9623), 1527-1537. doi:10.1016/s0140-6736(08)60658-3
- Weinstein, S. L., Dolan, L. A., Wright, J. G., & Dobbs, M. B. (2013). Effects of bracing in adolescents with idiopathic scoliosis. *N Engl J Med*, 369(16), 1512-1521. doi:10.1056/NEJMoal307337
- Wise, C. A., Sepich, D., Ushiki, A., Khanshour, A. M., Kidane, Y. H., Makki, N., . . . Solnica-Krezel, L. (2020). The cartilage matrisome in adolescent idiopathic scoliosis. *Bone Research*, 8(1). doi:10.1038/s41413-020-0089-0